



Figure 1 Location of Fox Island Laboratory

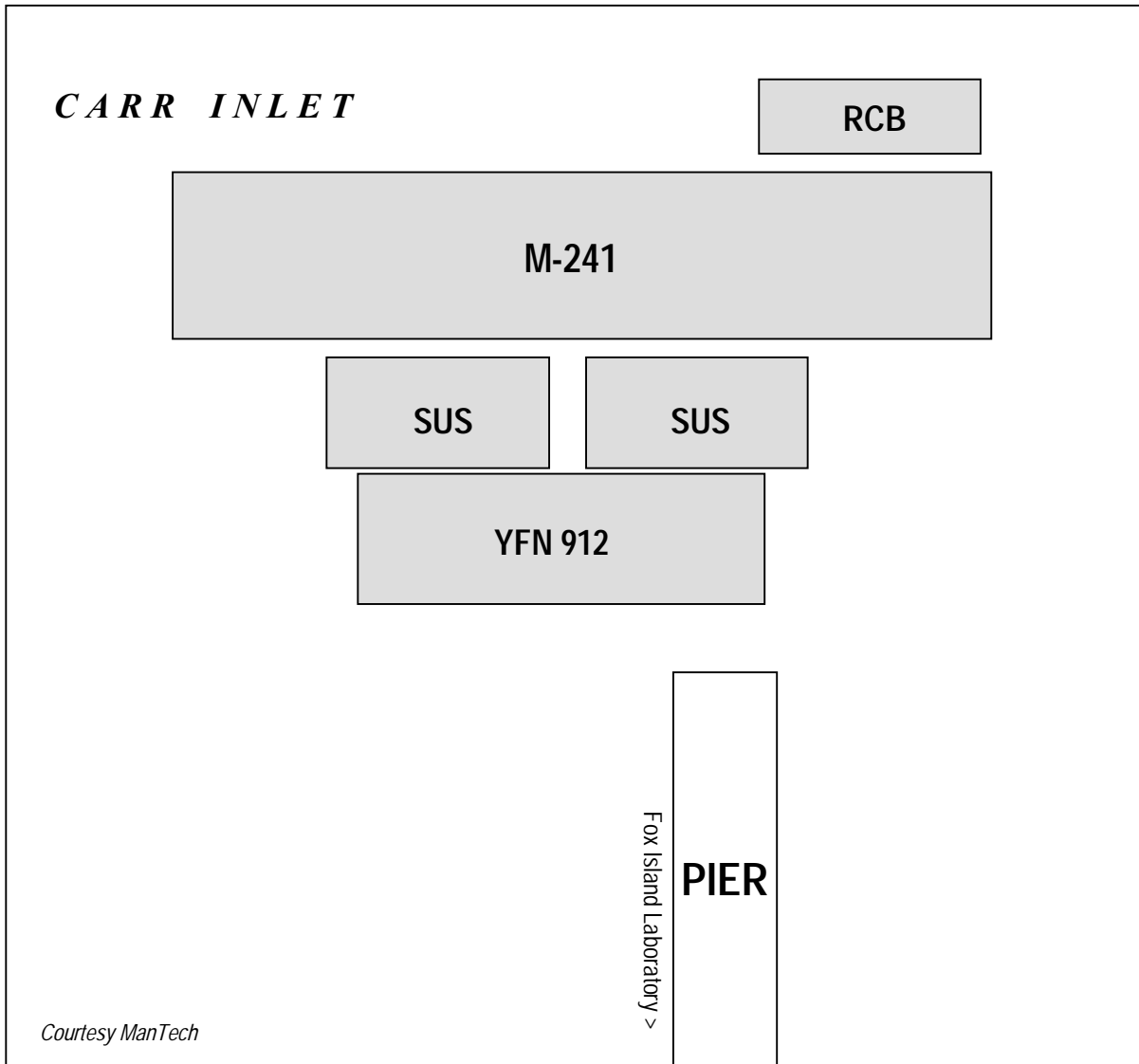


Figure 2 Configuration of barges at FIL on July 8, 2002



Figure 3 FIL pier and barges viewed from the northwest

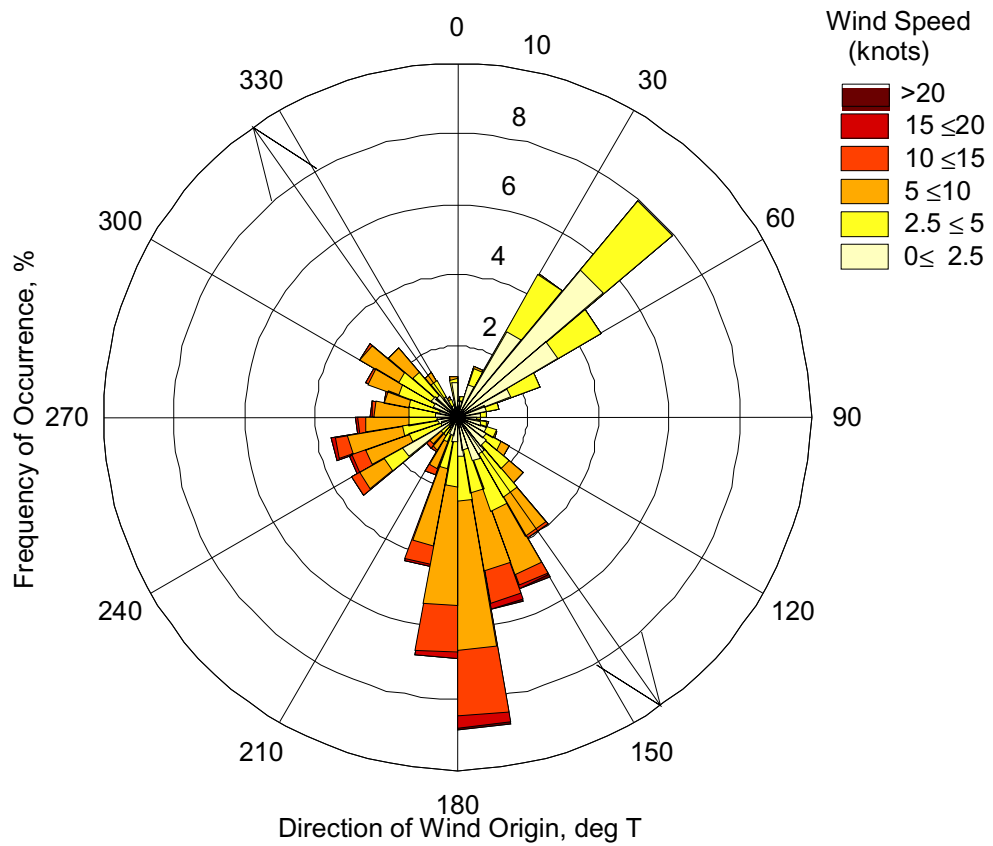


Figure 4 Wind rose of hourly wind measurements at FIL between October 29, 1999 and July 30, 2002
 Note: The arrow shows the shoreline orientation



Figure 5 Example bulkhead structures northwest of FIL

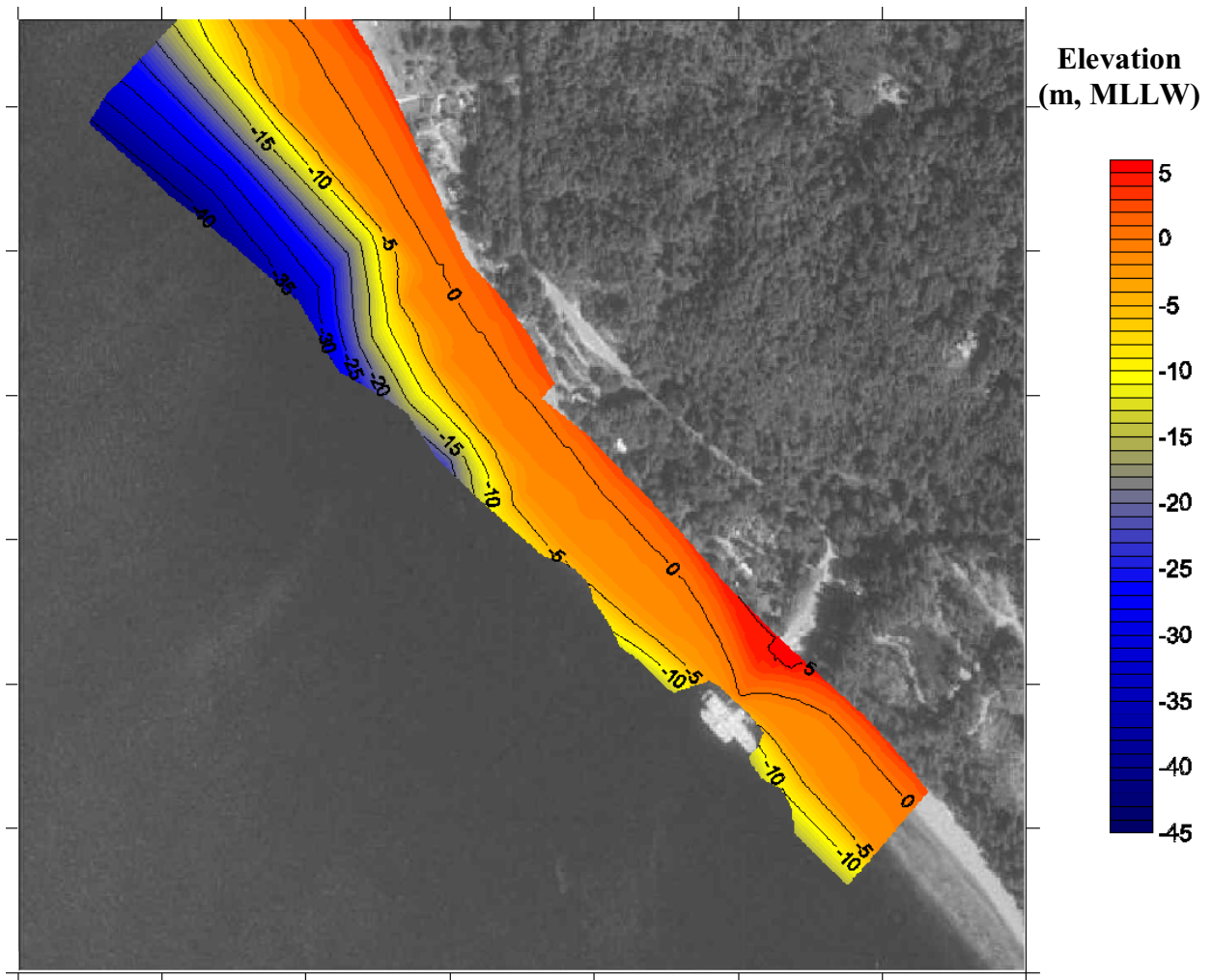


Figure 6 Bathymetry contours based on 2002 survey superimposed on DOQ

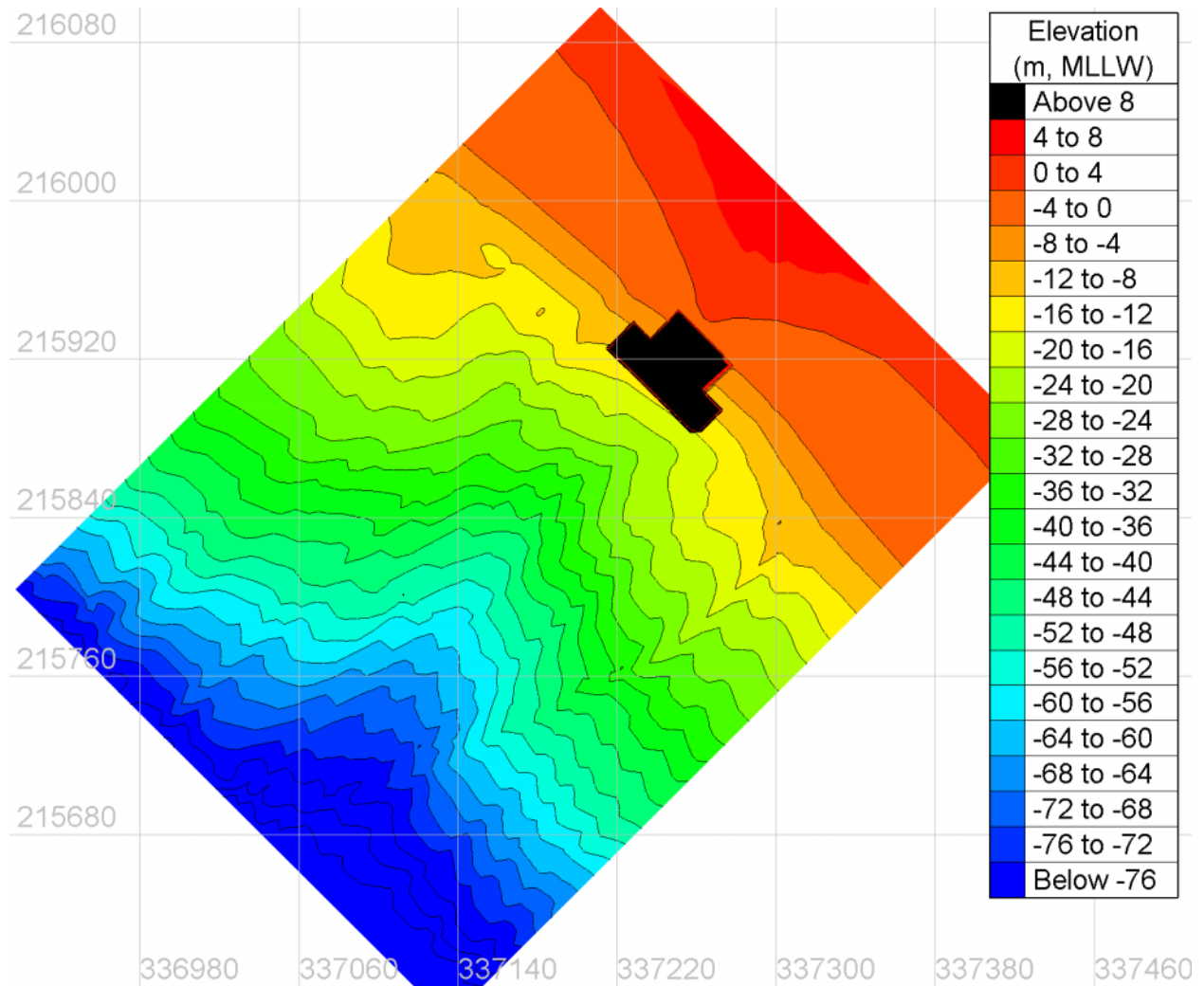


Figure 7 Composite bathymetry based on 2002 surveys showing location of FIL barges

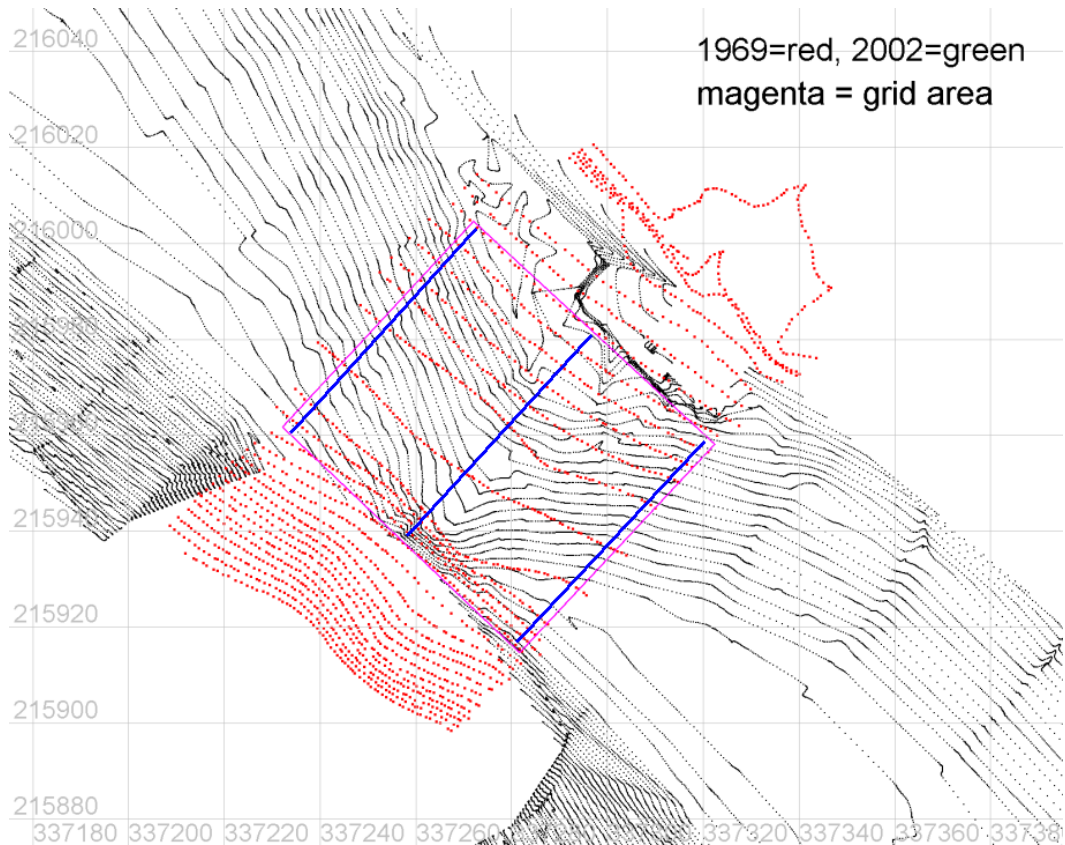


Figure 8 Comparison of 1969 and 2002 surveys showing region of overlap and profile transects

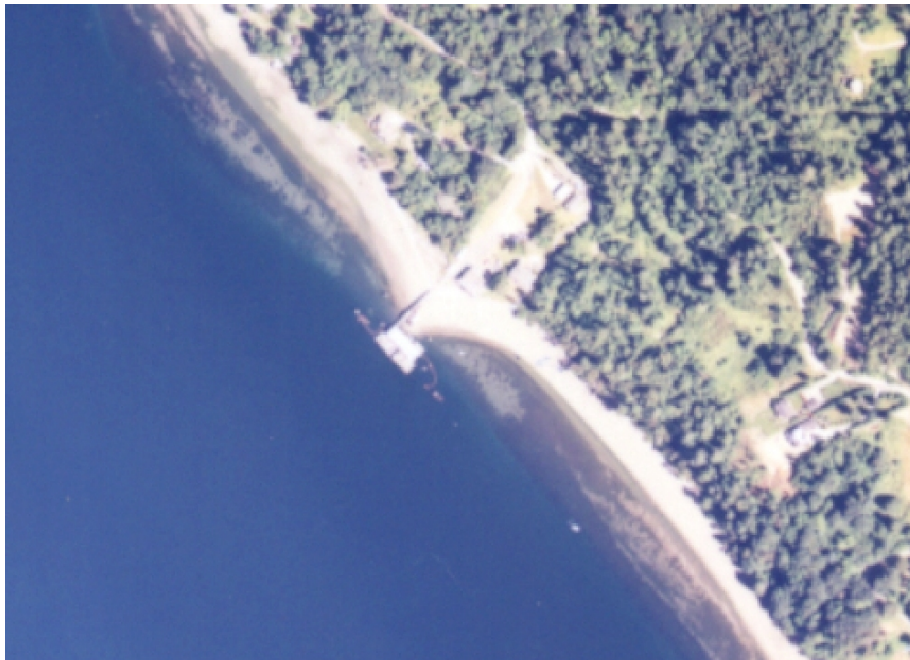
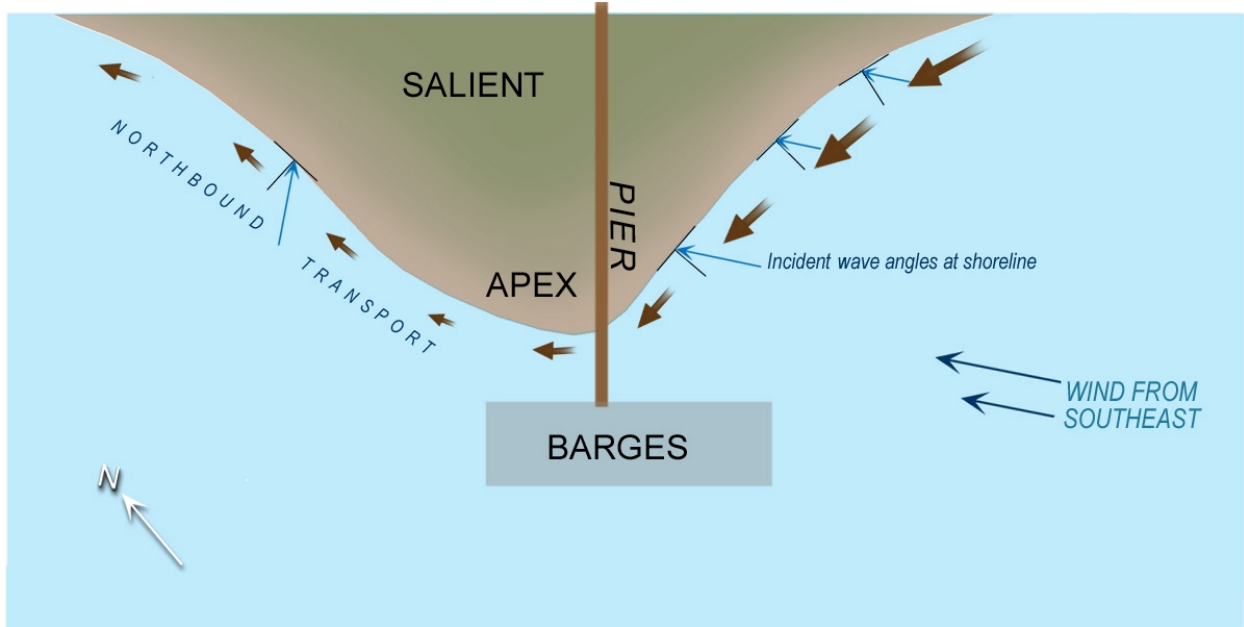
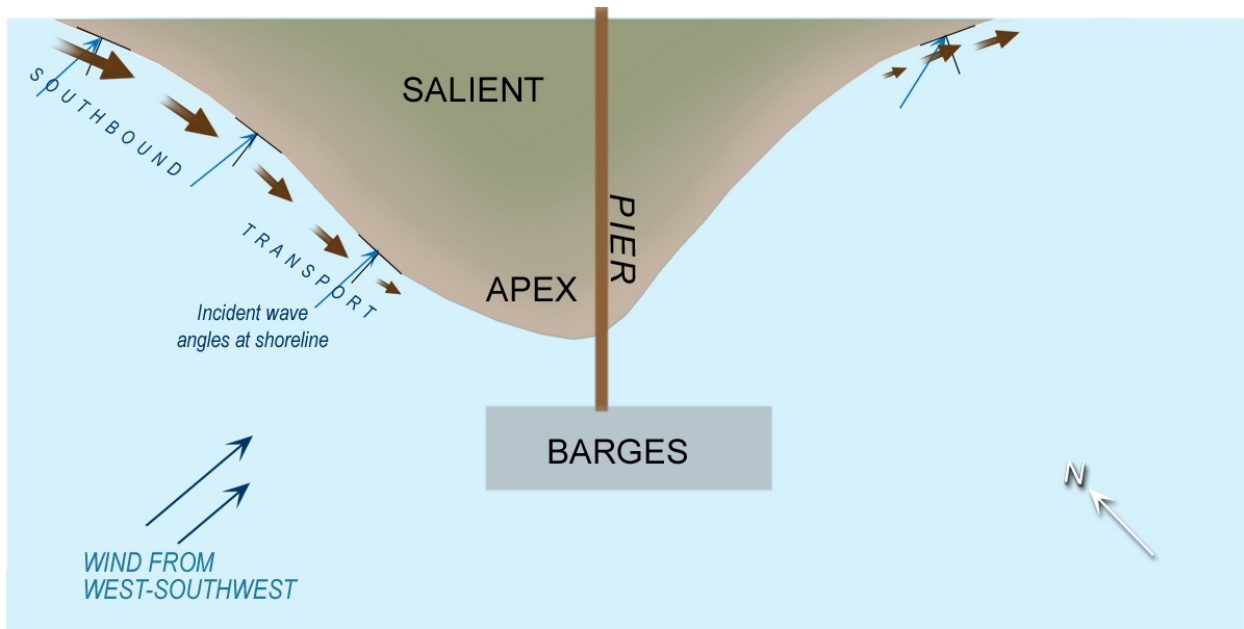


Figure 9 Aerial photograph of FIL facility (2001) showing the north-south asymmetry of the salient



a



b

Figure 10 Conceptual schematics of transport patterns in response to varying angle of incident waves at the salient for waves from (a) the southeast, and (b) the west-southwest

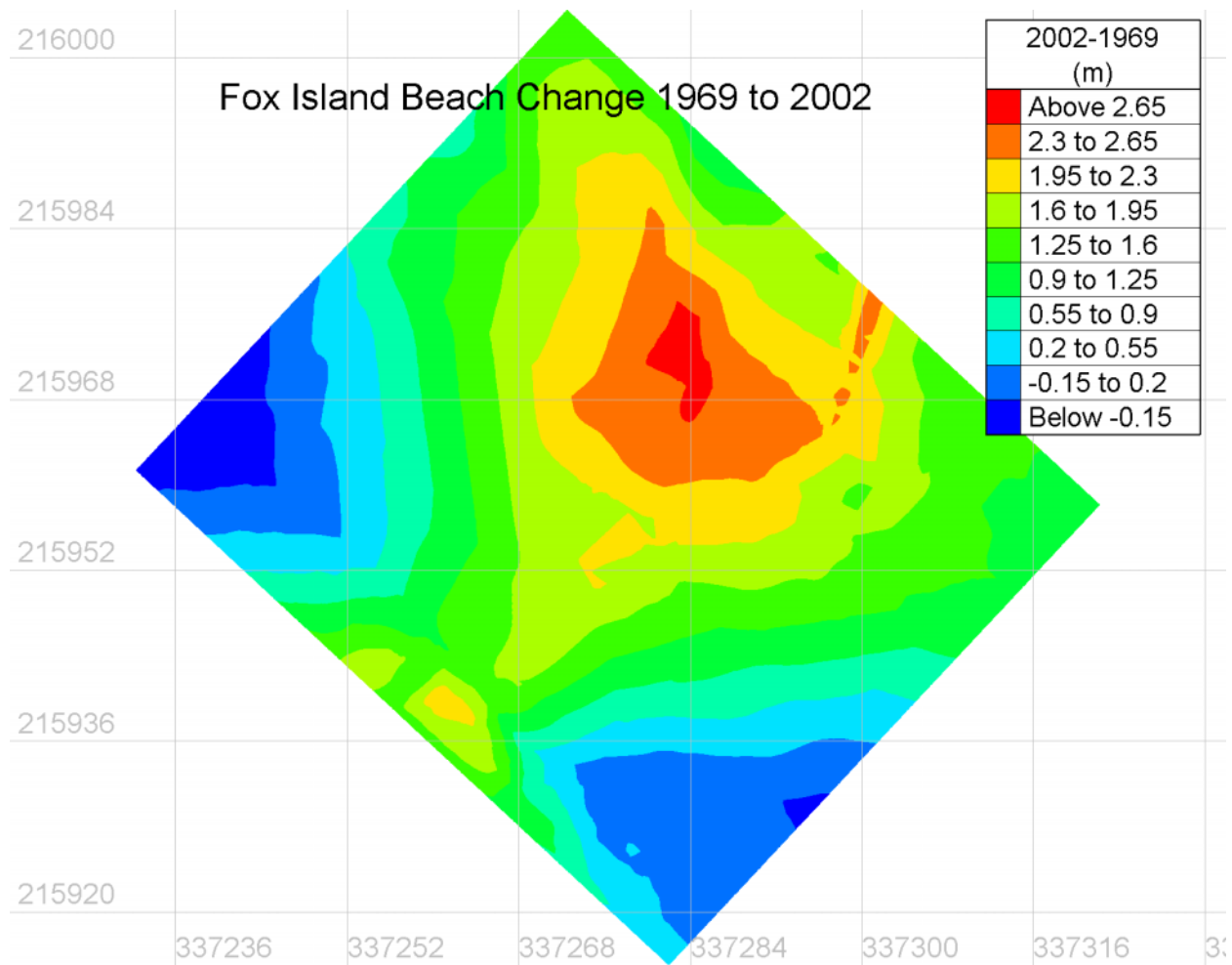


Figure 11 Map of vertical differences in Fox Island seabed elevation between 1969 and 2002 bathymetric surfaces

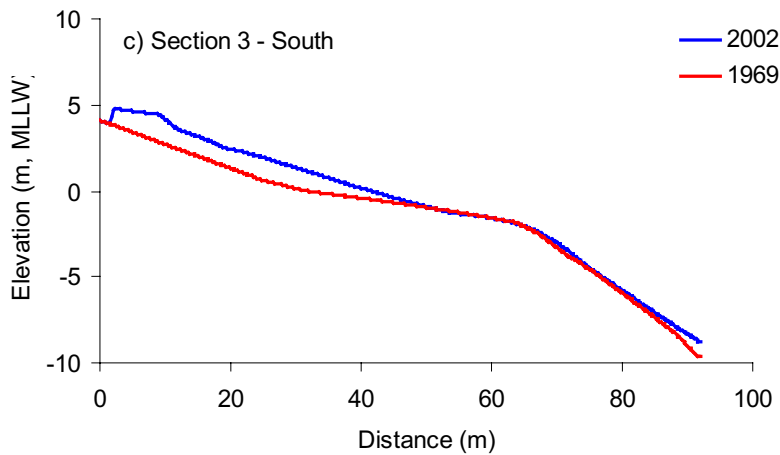
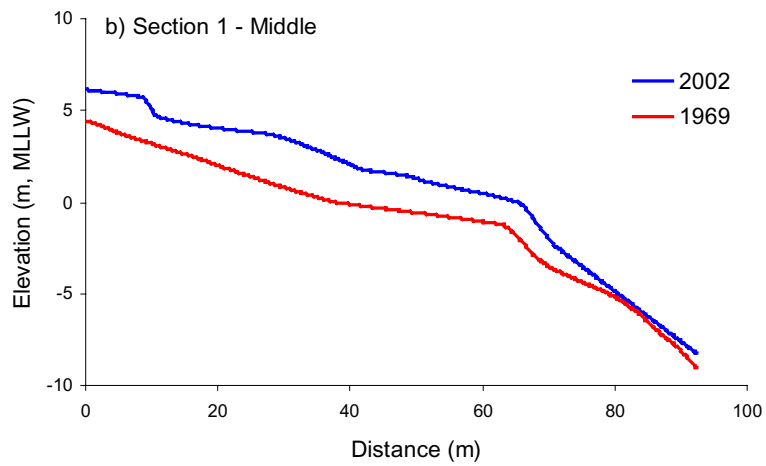
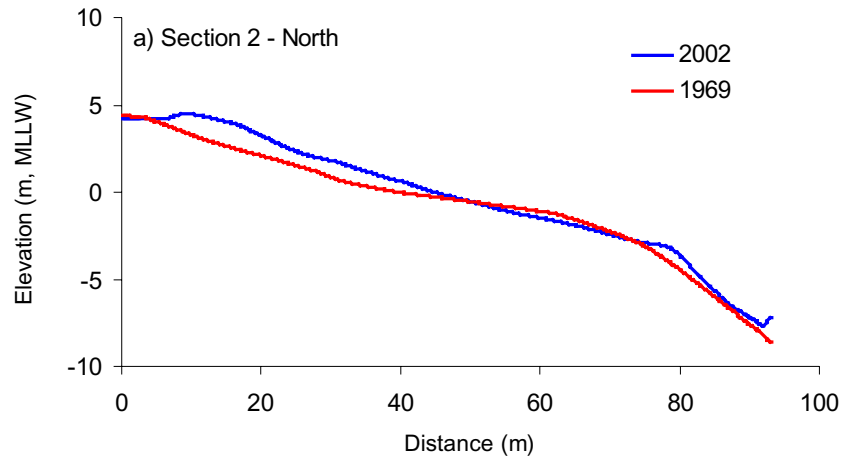


Figure 12 Comparison of bottom elevations for the 1969 and 2002 surveys along the three transects shown in Figure 8

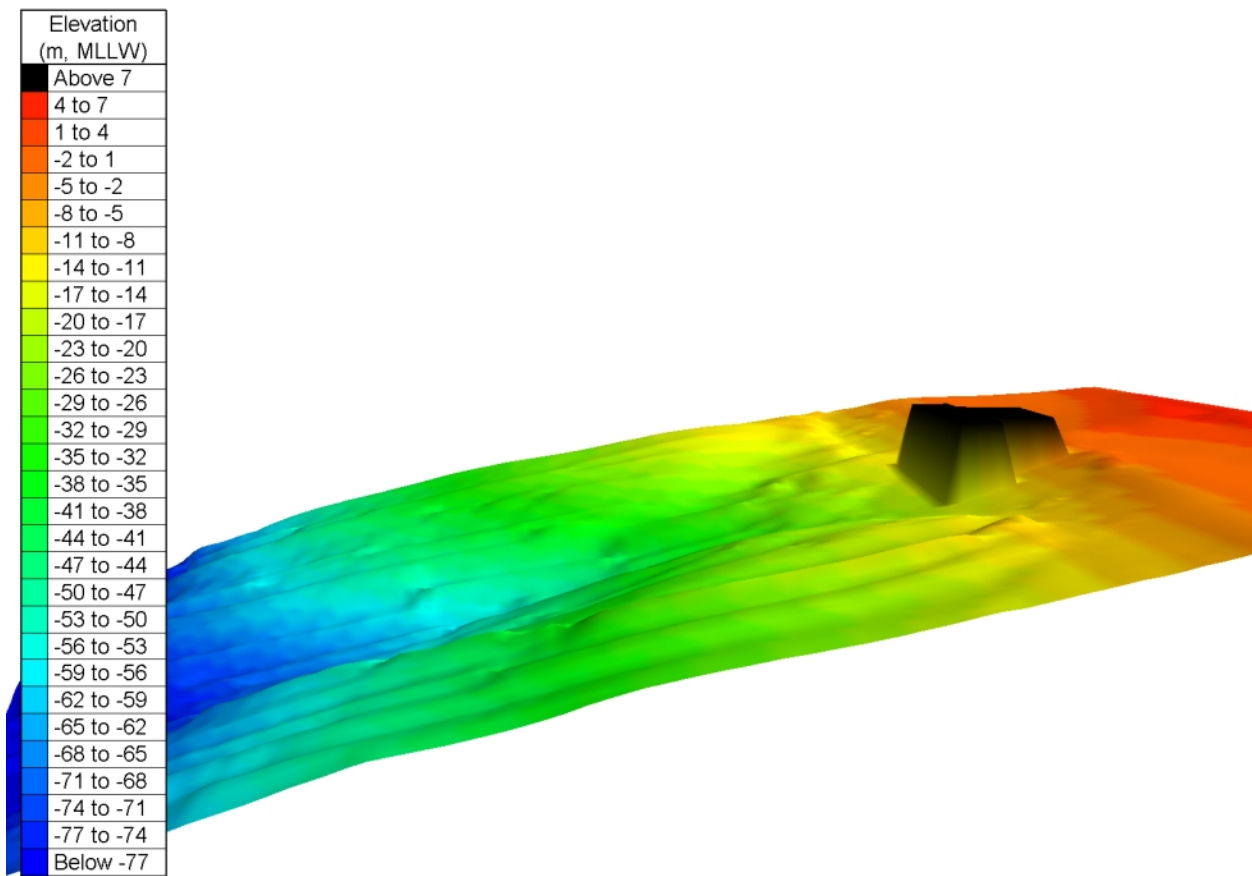


Figure 13 Three-dimensional visualization of the 2002 bathymetry

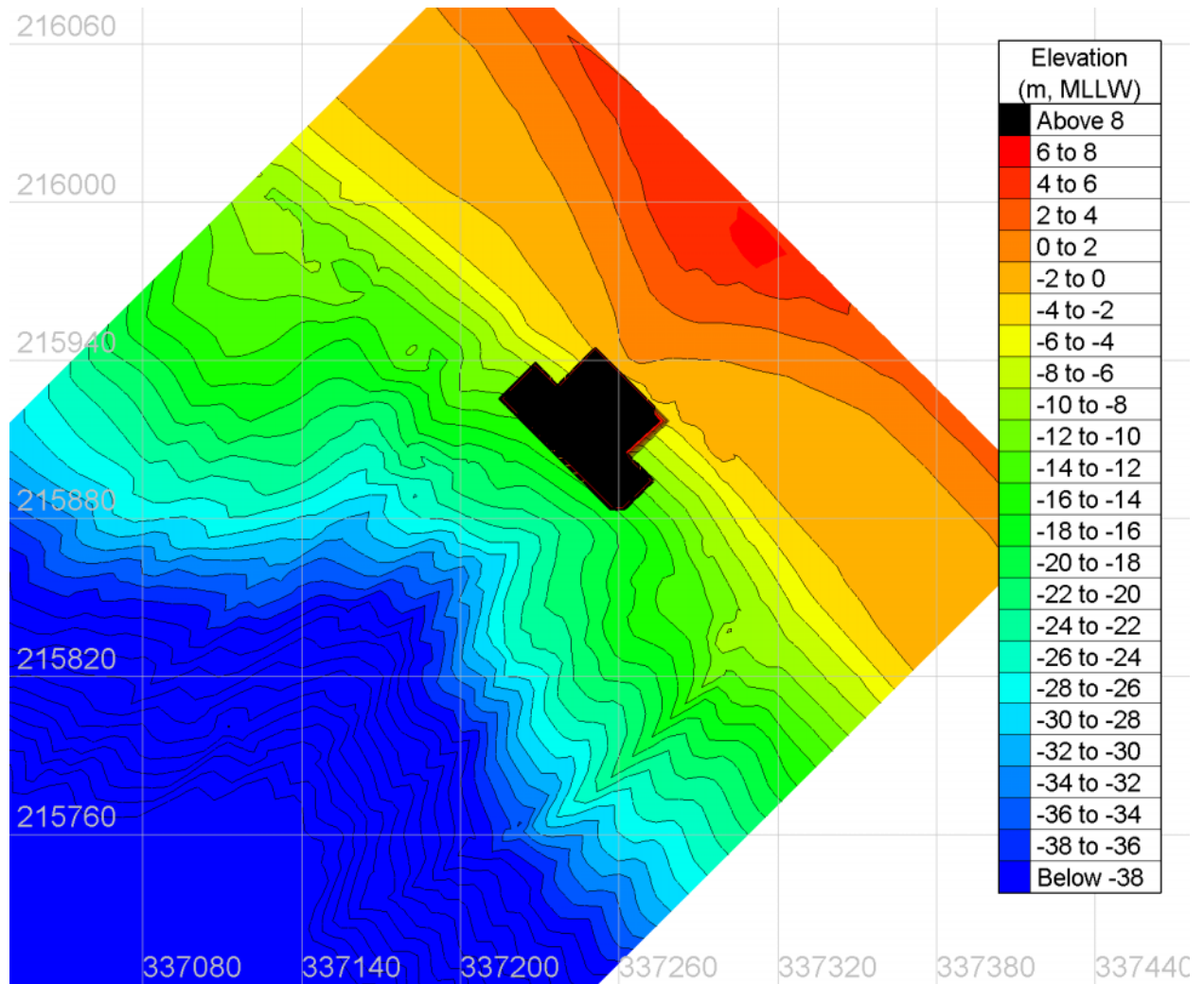


Figure 14 Close-up of the 2002 bathymetry near the FIL

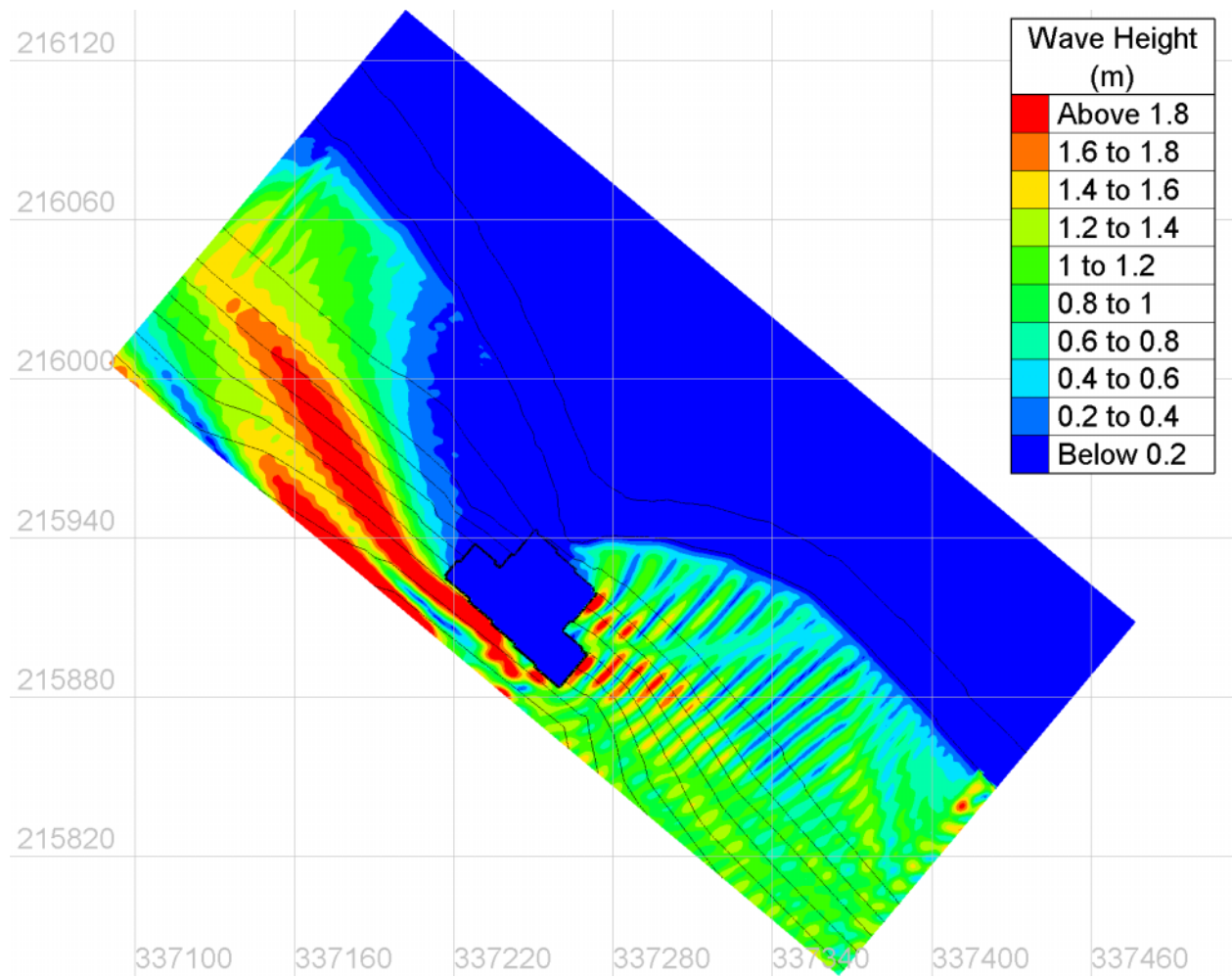


Figure 15 Spatial distribution of wave heights simulated with the COASTOX model for incident waves with DIR = 170 deg, Tide = 0.0 m, H = 1.0 m, T = 3 sec

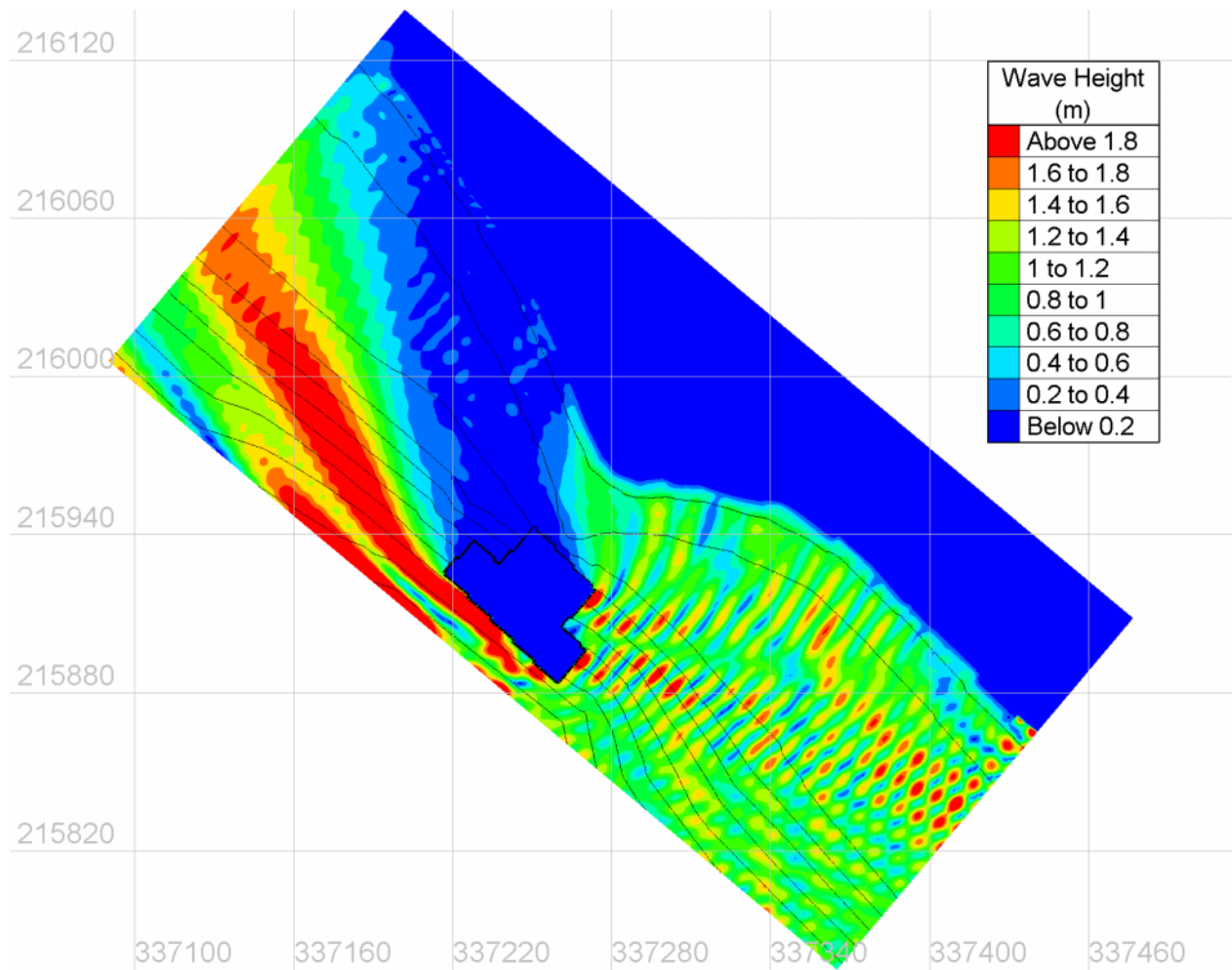


Figure 16 Spatial distribution of wave heights simulated with the COASTOX model for incident waves with DIR = 170 deg, Tide = 3.0 m, H = 1.0 m, T = 3 sec

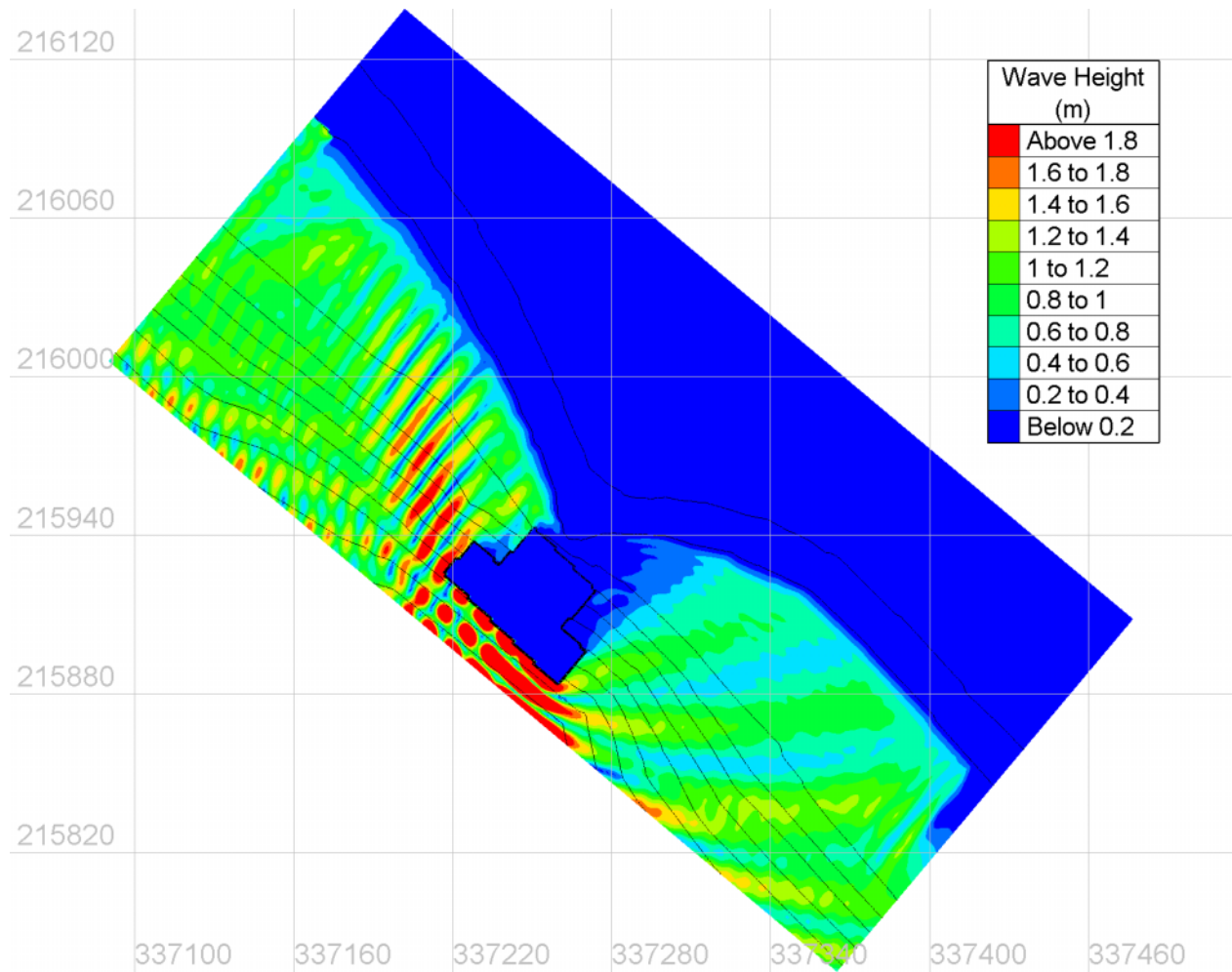


Figure 17 Spatial distribution of wave heights simulated with the COASTOX model for incident waves with DIR = 260 deg, Tide = 0.0 m, H = 1.0 m, T = 3 sec

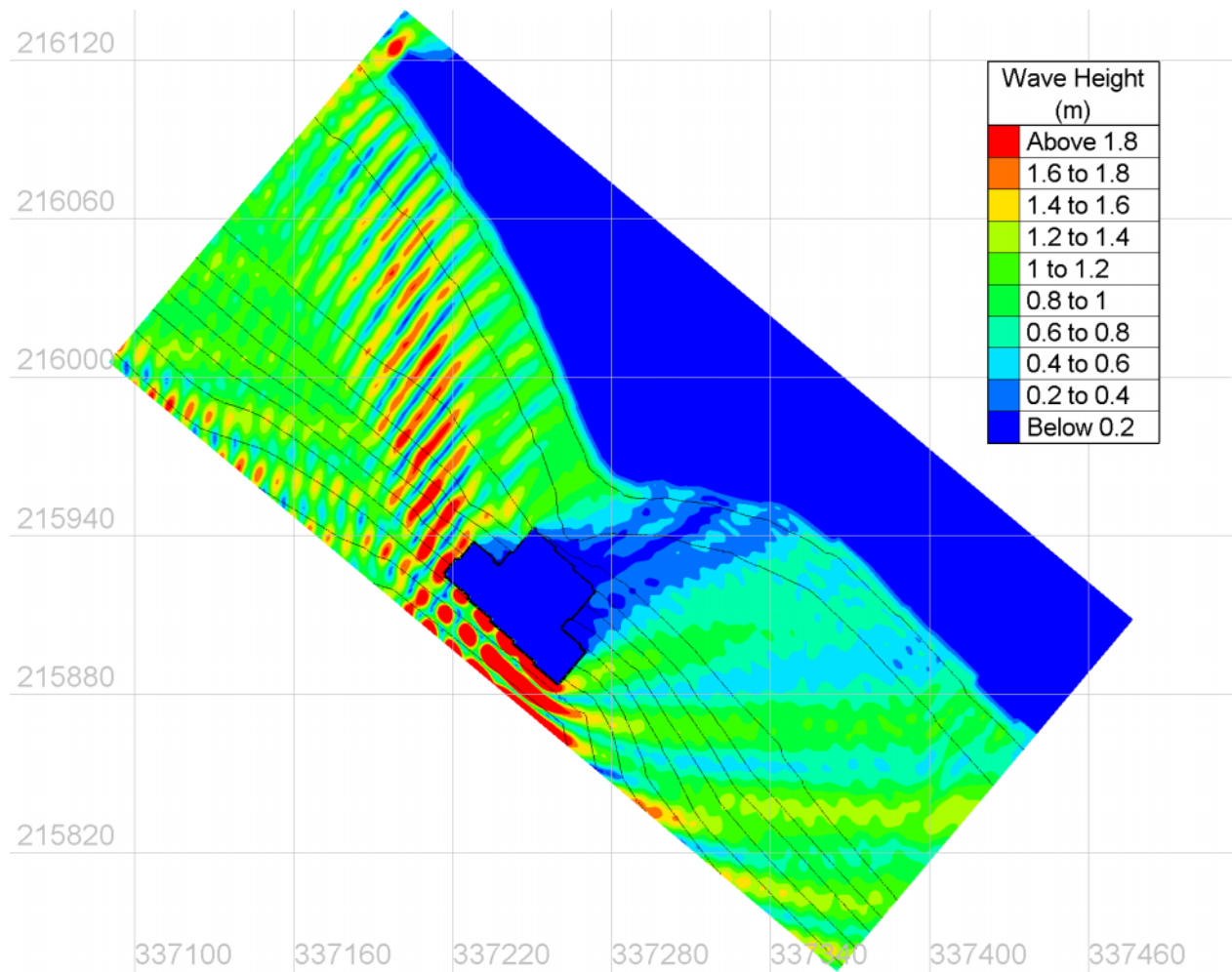


Figure 18 Spatial distribution of wave heights simulated with the COASTOX model for incident waves with DIR = 260 deg, Tide = 3.0 m, H = 1.0 m, T = 3 sec

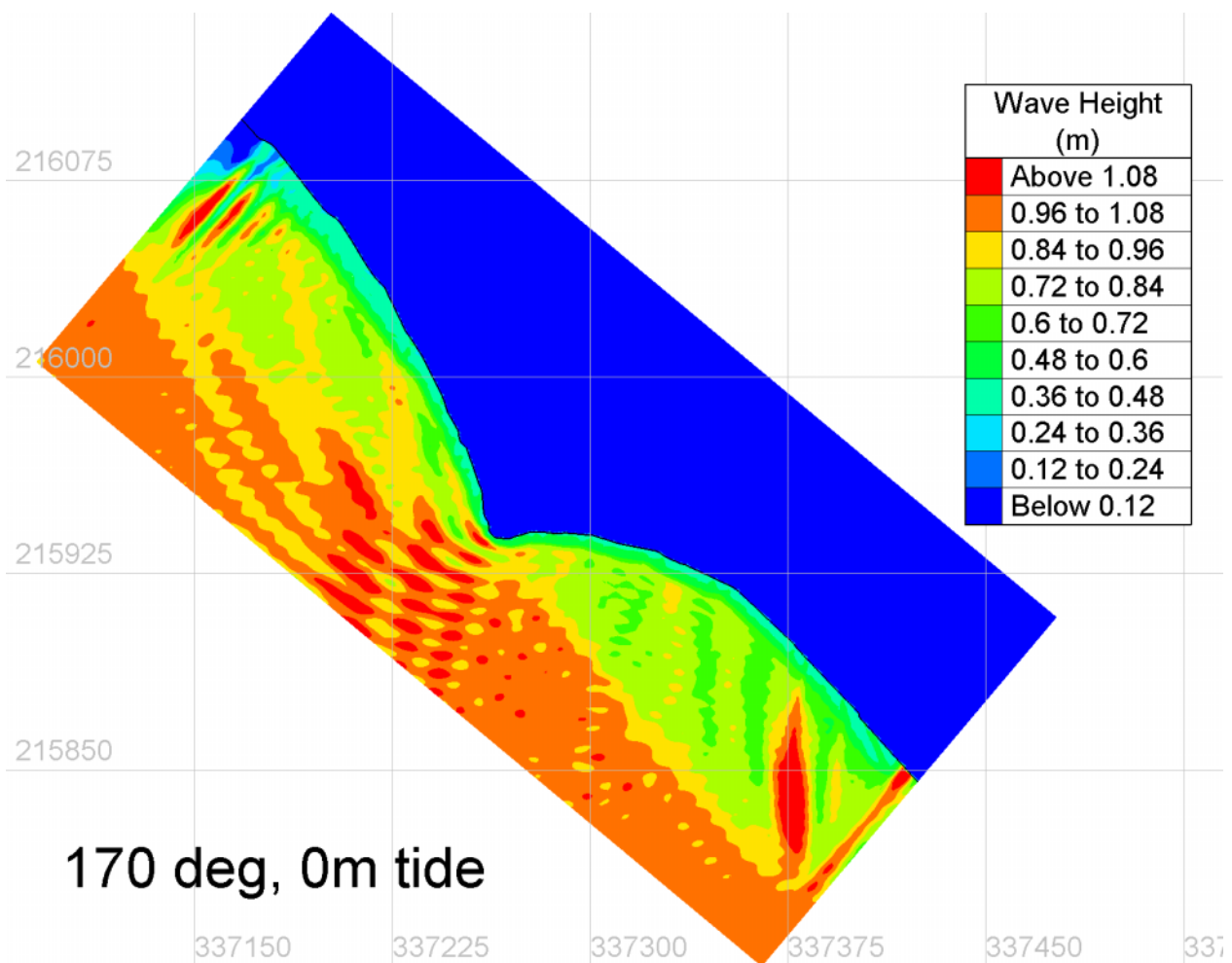


Figure 19 Spatial distribution of wave heights simulated with the COASTOX model for incident waves with DIR = 170 deg, Tide = 0.0 m, H = 1.0 m, T = 3 sec, with no barges present

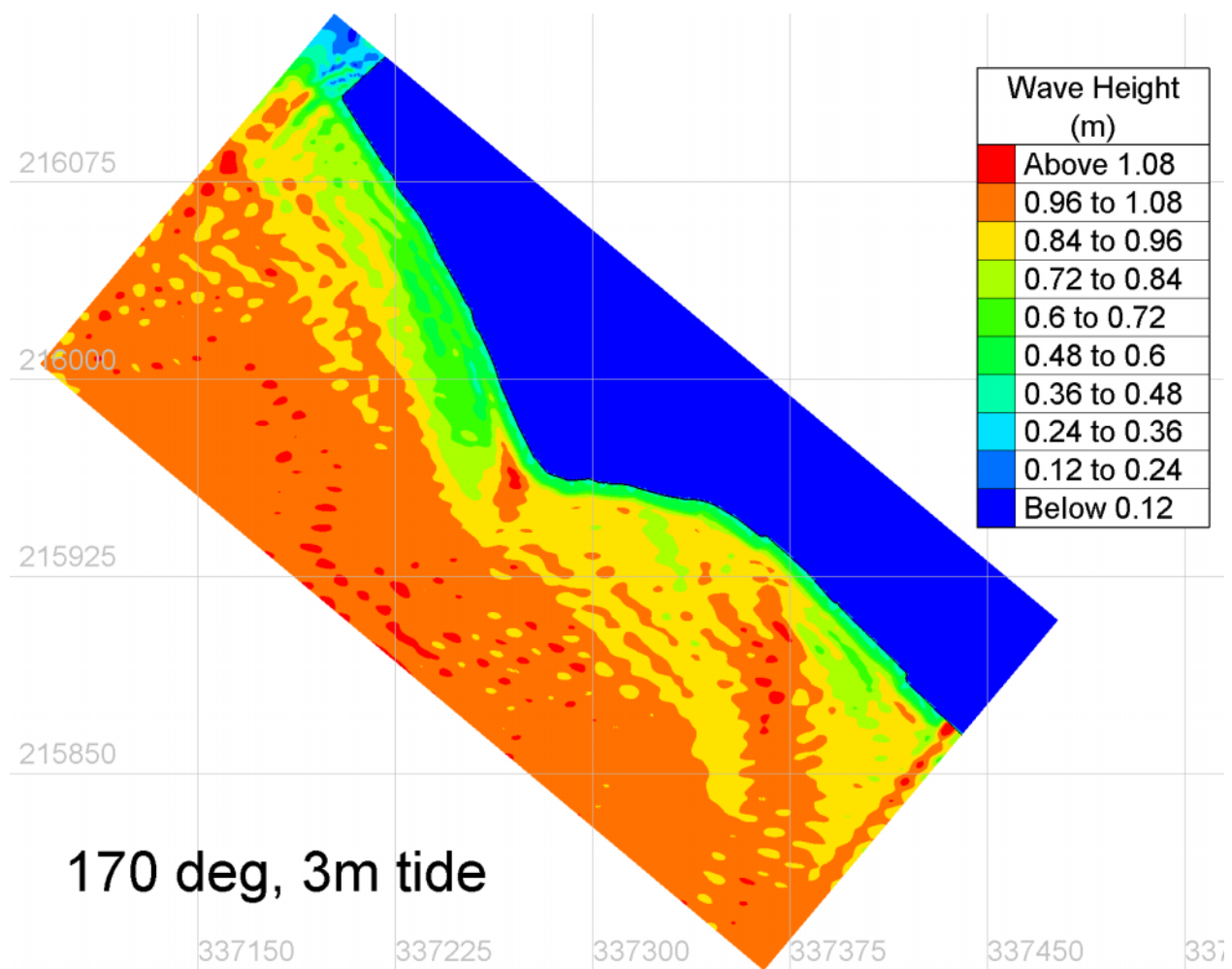


Figure 20 Spatial distribution of wave heights simulated with the COASTOX model for incident waves with DIR = 170 deg, Tide = 3.0 m, H = 1.0 m, T = 3 sec, with no barges present

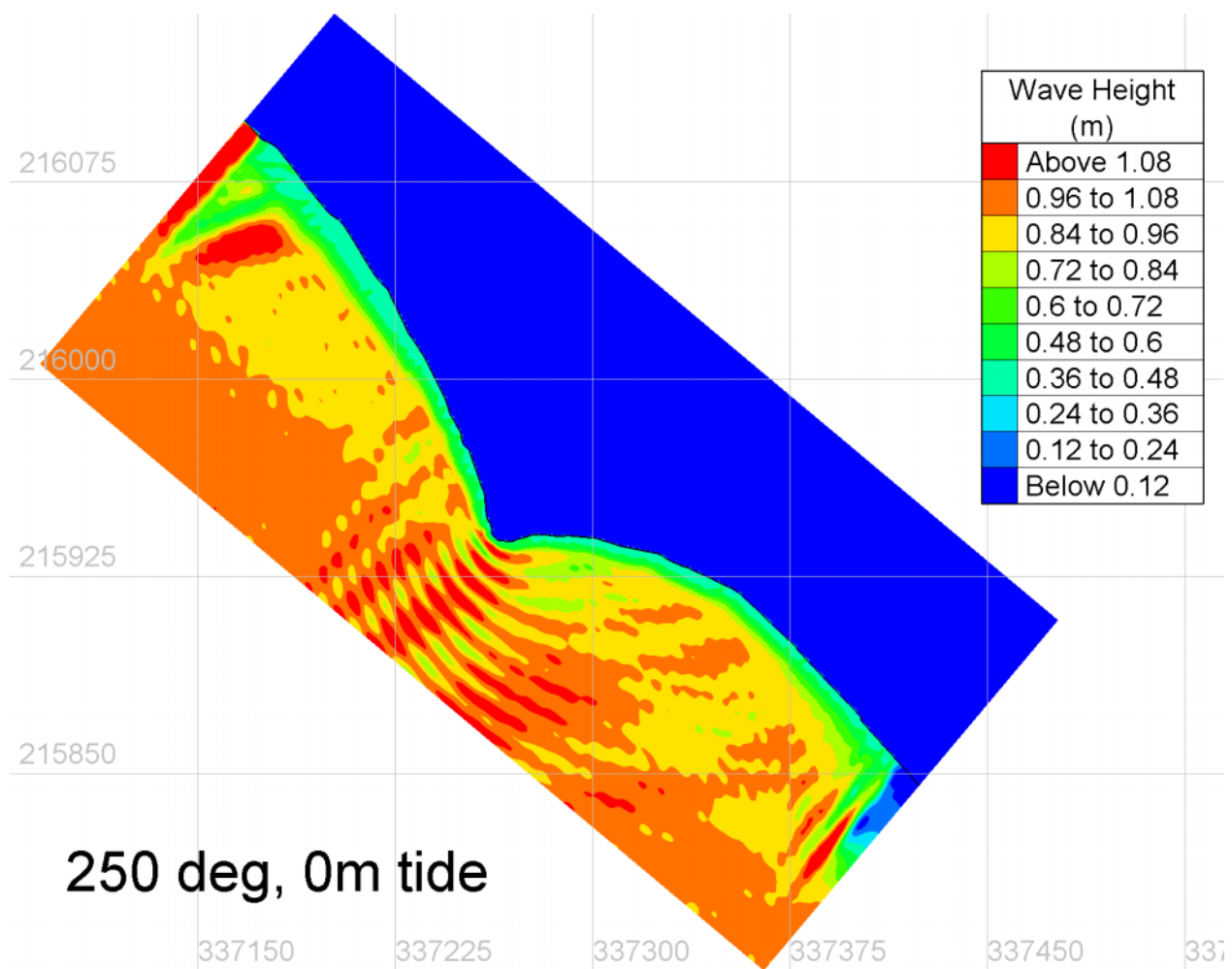


Figure 21 Spatial distribution of wave heights simulated with the COASTOX model for incident waves with DIR = 250 deg, Tide = 0.0 m, H = 1.0 m, T = 3 sec, with no barges present

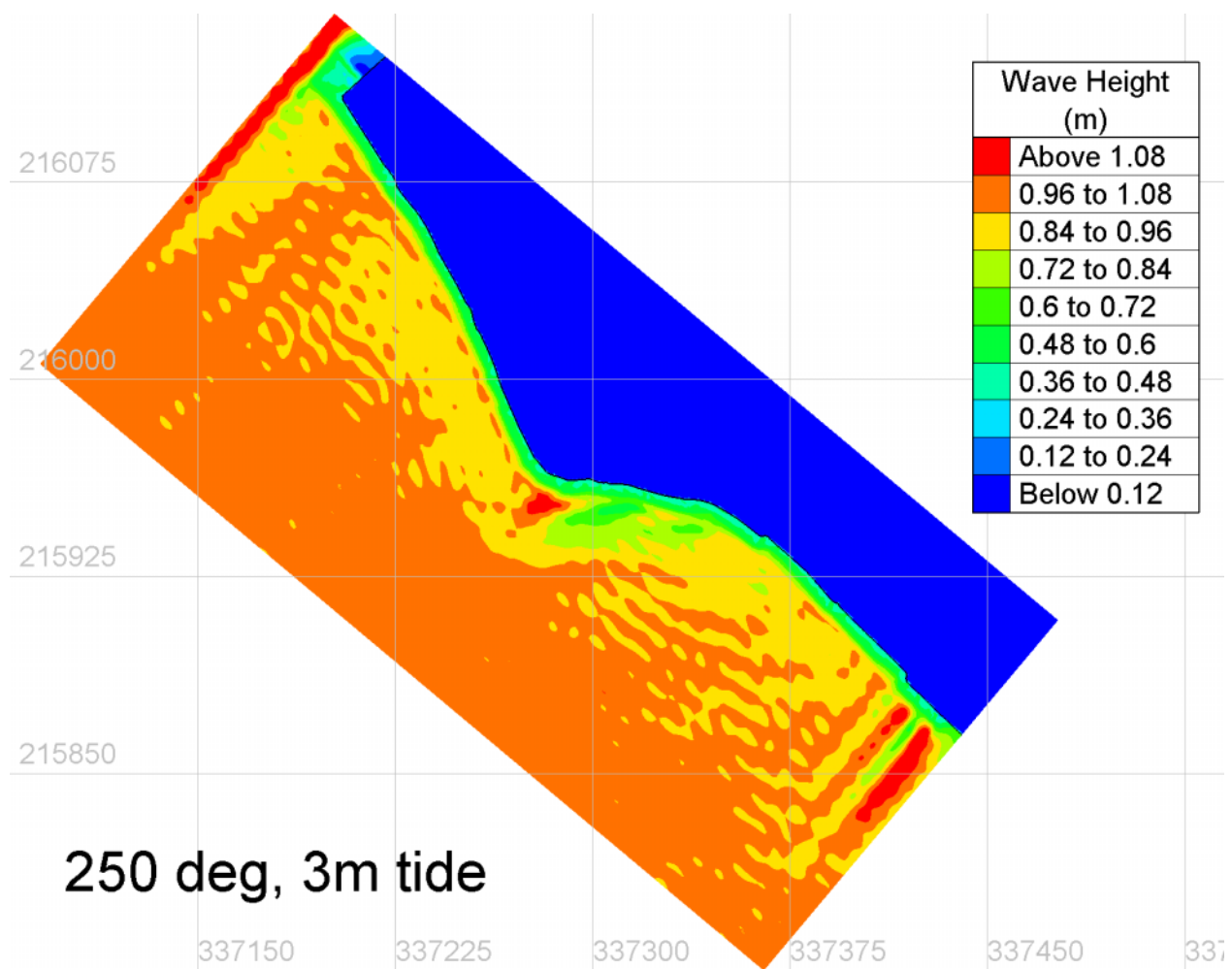


Figure 22 Spatial distribution of wave heights simulated with the COASTOX model for incident waves with DIR = 250 deg, Tide = 3.0 m, H = 1.0 m, T = 3 sec, with no barges present

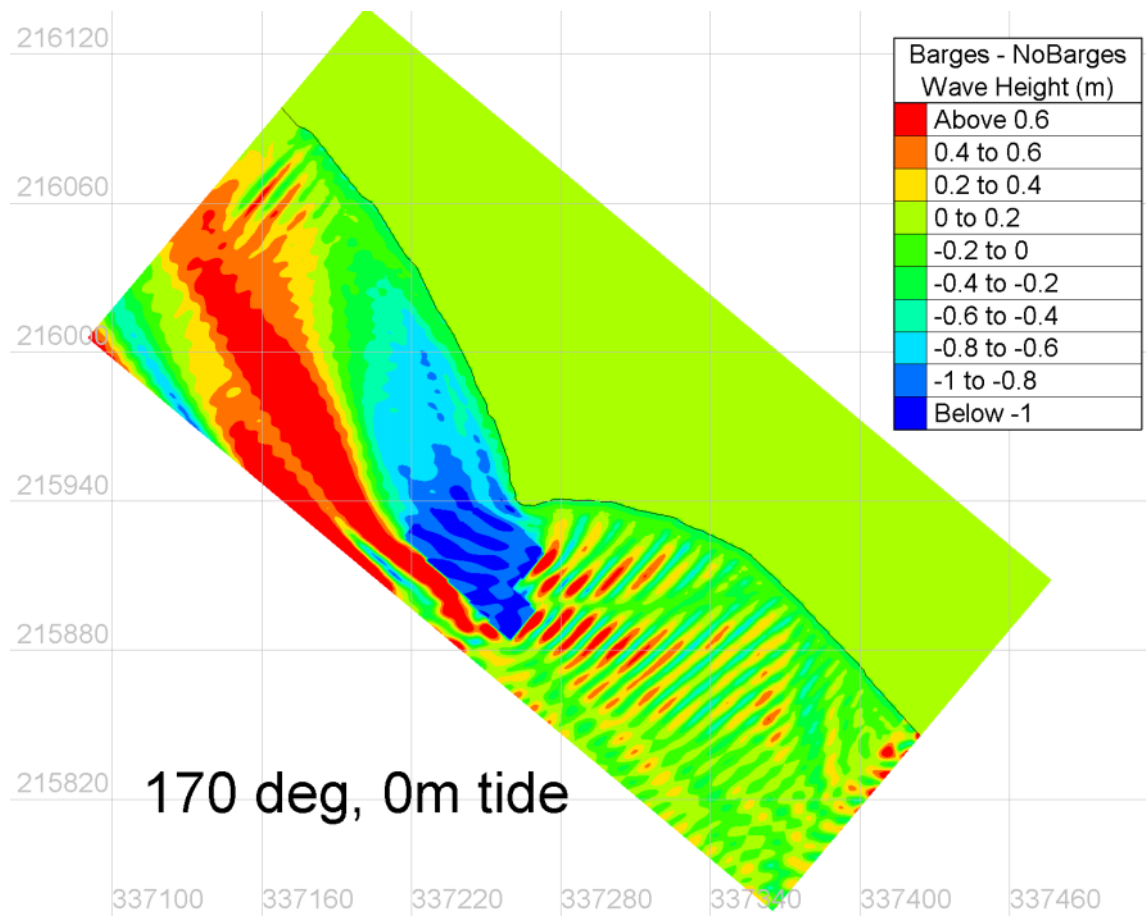


Figure 23 Spatial distribution of wave height differences between the simulation with barges present and no barges present by the COASTOX model for incident waves with DIR = 170 deg, Tide = 0.0 m, H = 1.0 m, T = 3 sec

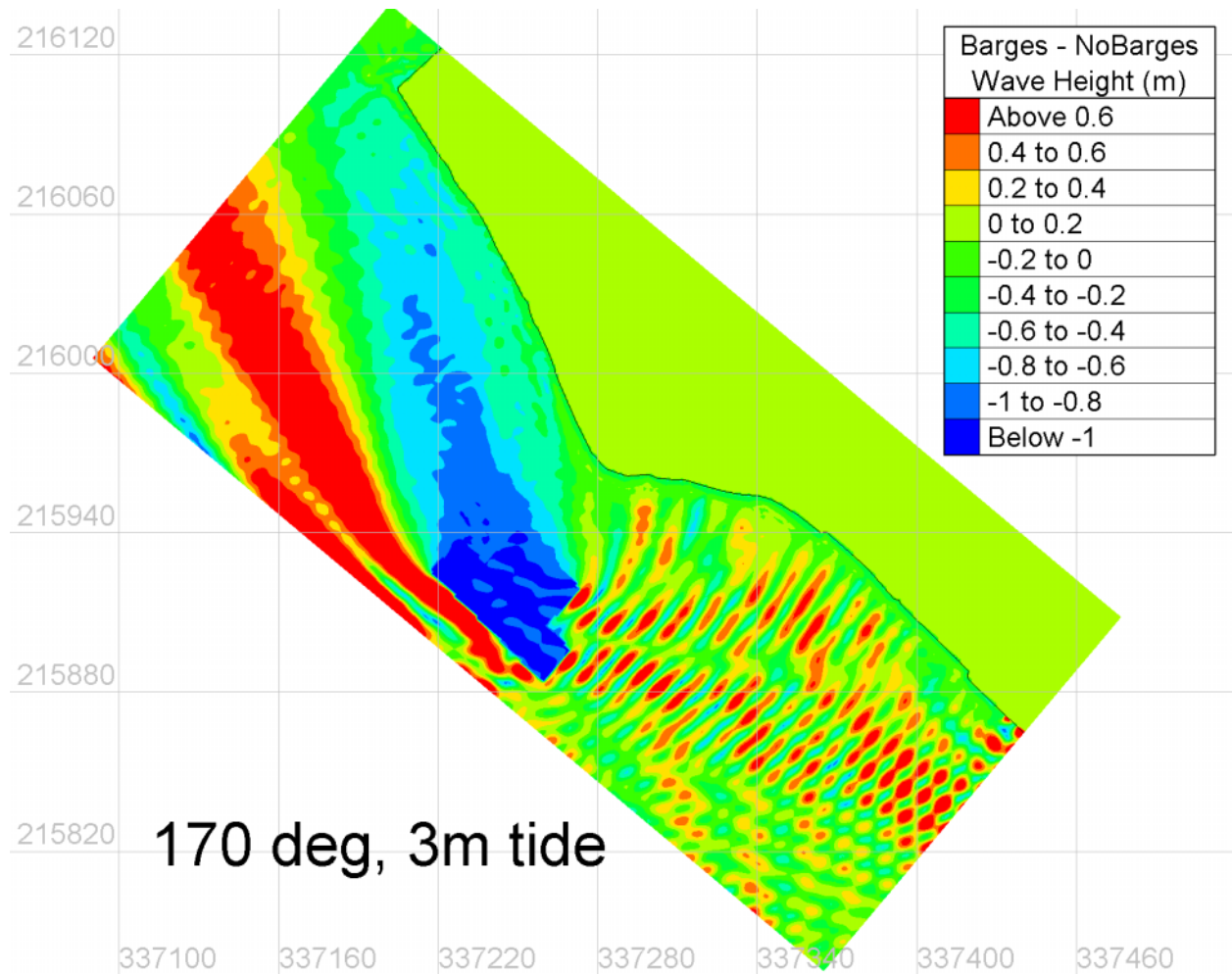


Figure 24 Spatial distribution of wave height differences between the simulation with barges present and no barges present by the COASTOX model for incident waves with DIR = 170 deg, Tide = 3.0 m, H = 1.0 m, T = 3 sec

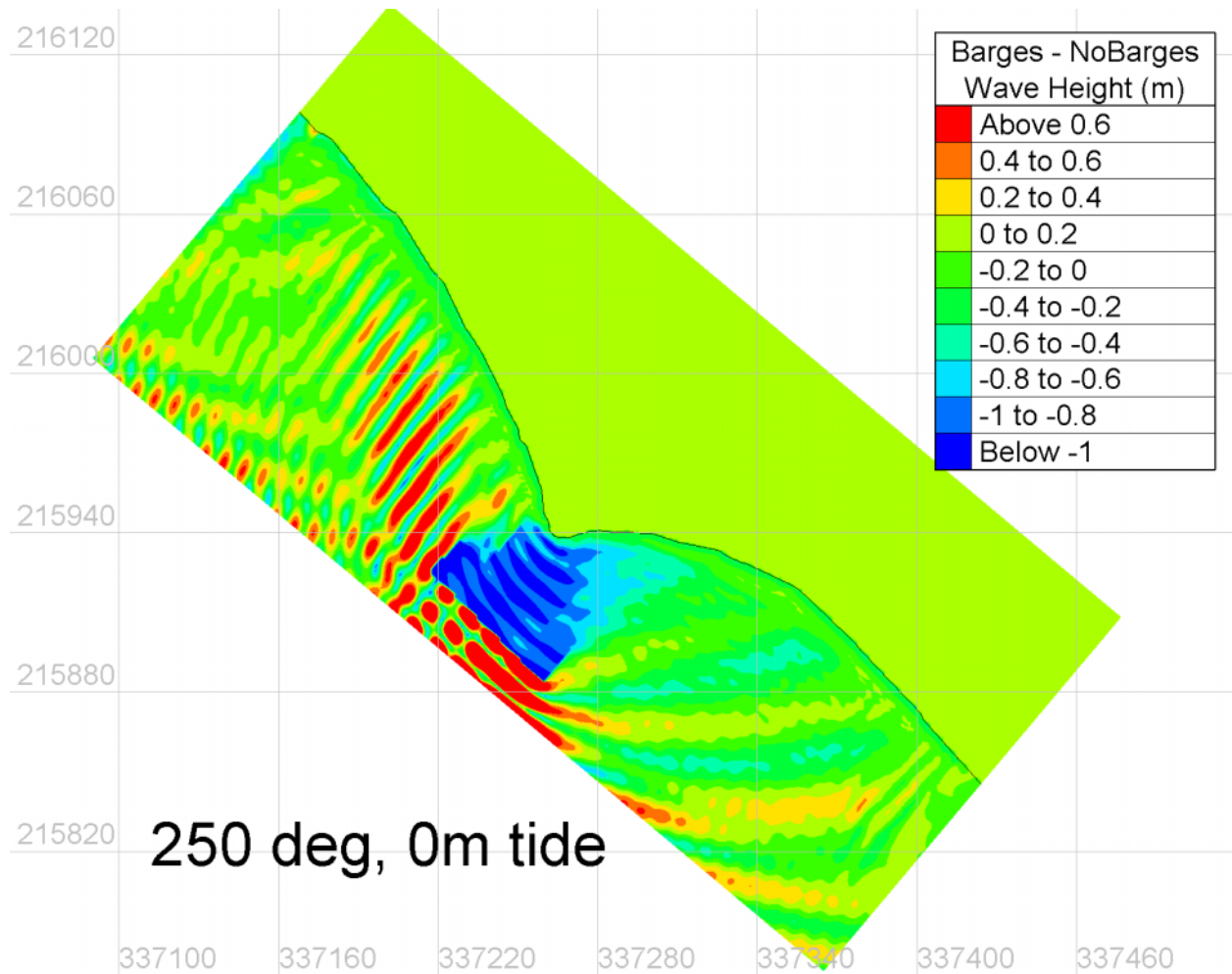


Figure 25 Spatial distribution of wave height differences between the simulation with barges present and no barges present by the COASTOX model for incident waves with DIR = 250 deg, Tide = 0.0 m, H = 1.0 m, T = 3 sec

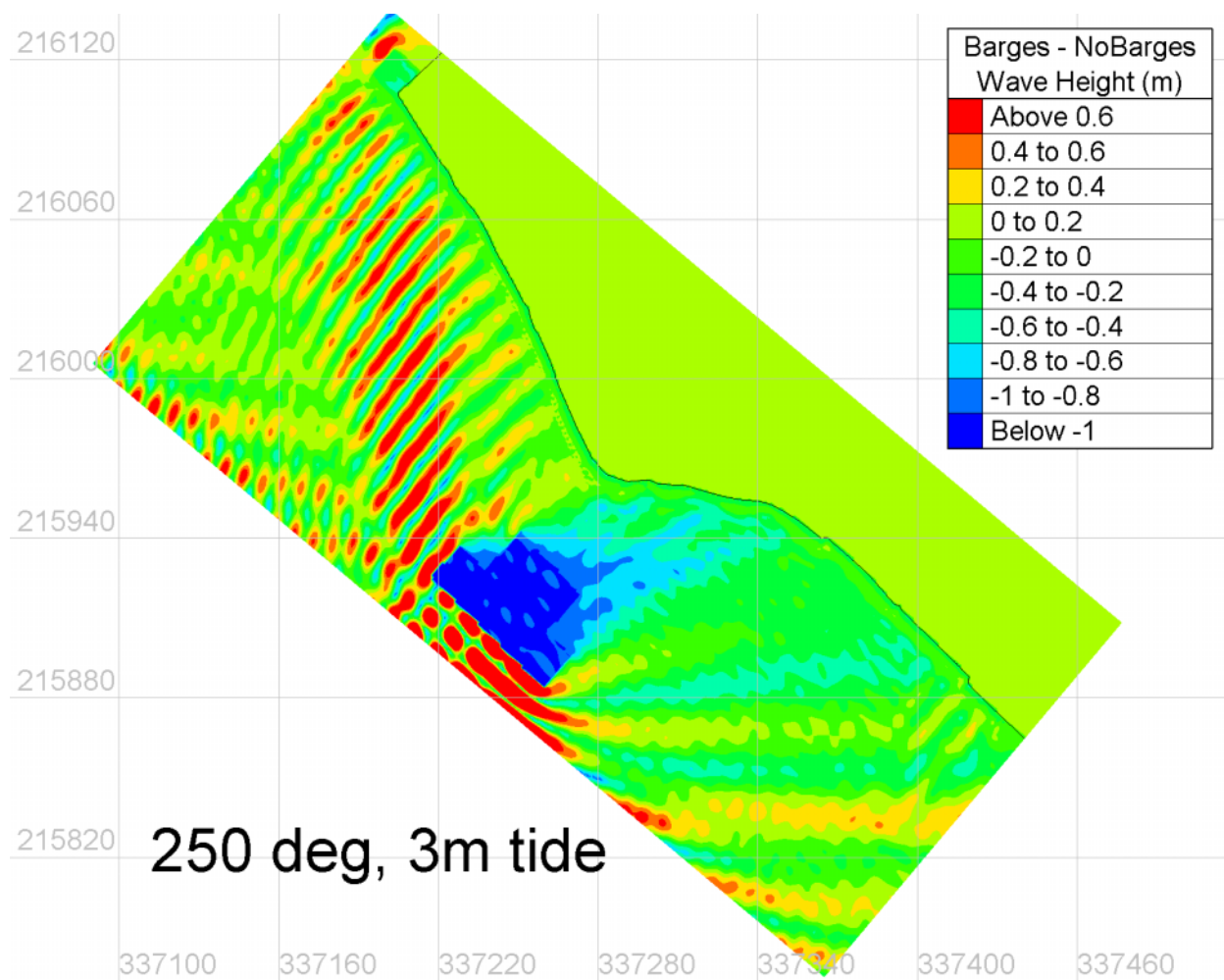


Figure 26 Spatial distribution of wave height differences between the simulation with barges present and no barges present by the COASTOX model for incident waves with DIR = 250 deg, Tide = 3.0 m, H = 1.0 m, T = 3 sec

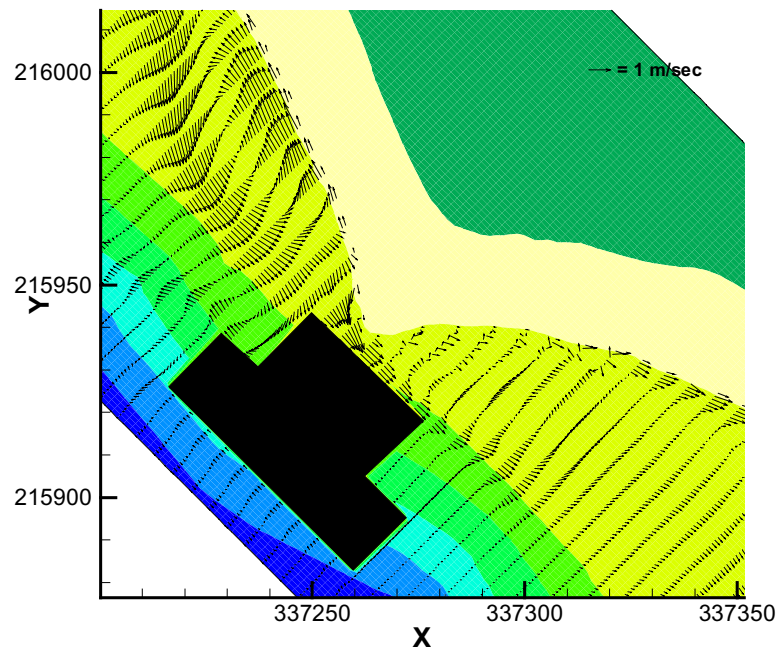
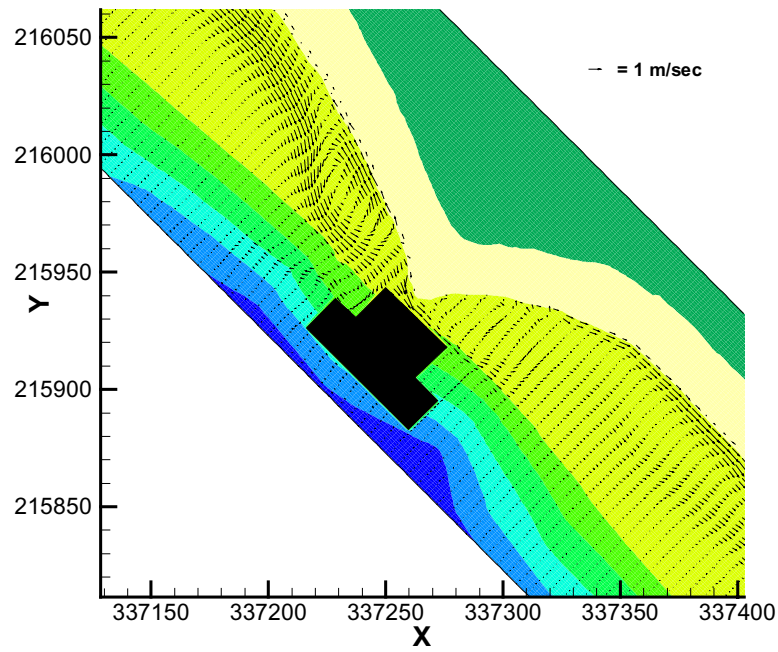


Figure 27 CoastL modeling of wave generated currents, for waves with DIR = 250 deg, H = 1 m, T = 3 sec, Tide = 0.0 m; (top) Large modeling area; (bottom) Close-up of FIL

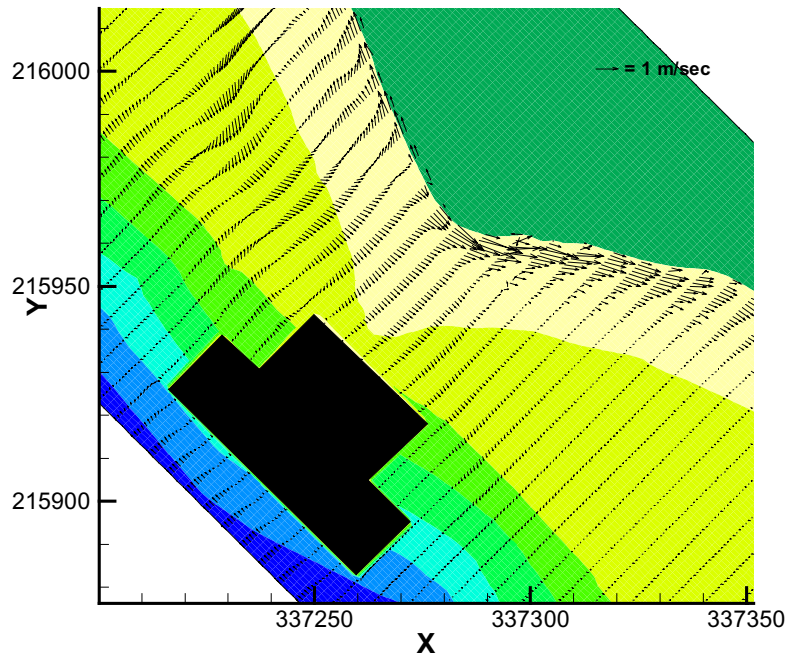
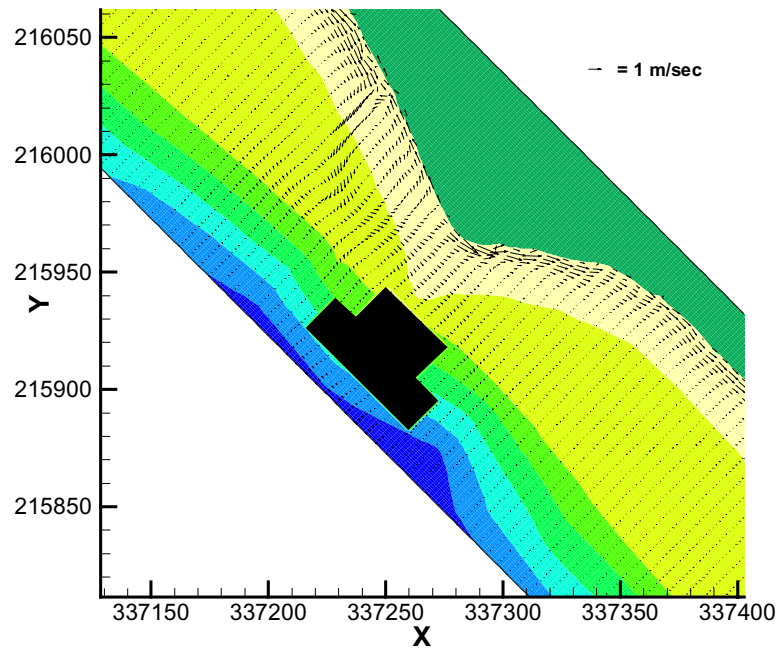


Figure 28 CoastL modeling of wave generated currents, for waves with DIR = 250 deg, H = 1 m, T = 3 sec, Tide = 3.0 m; (top) Large modeling area; (bottom) Close-up of FIL

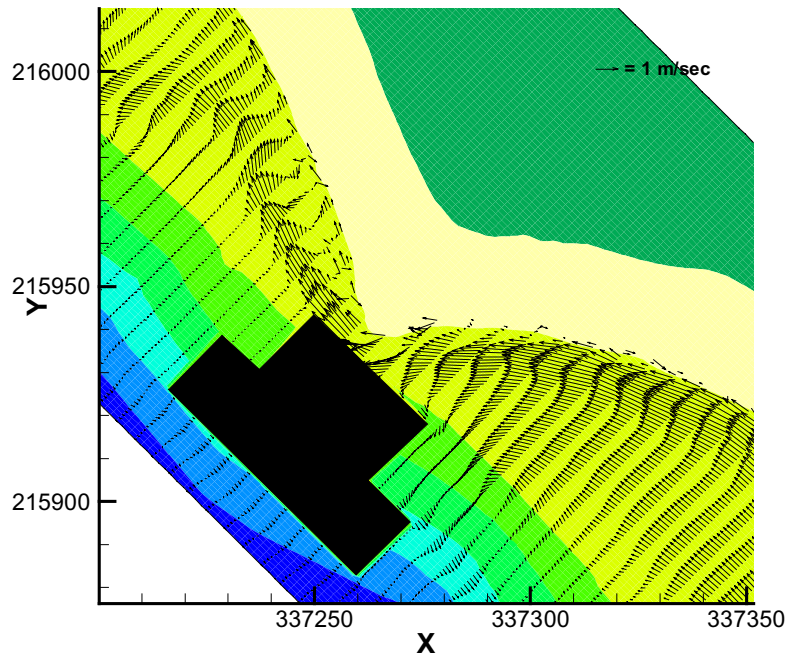
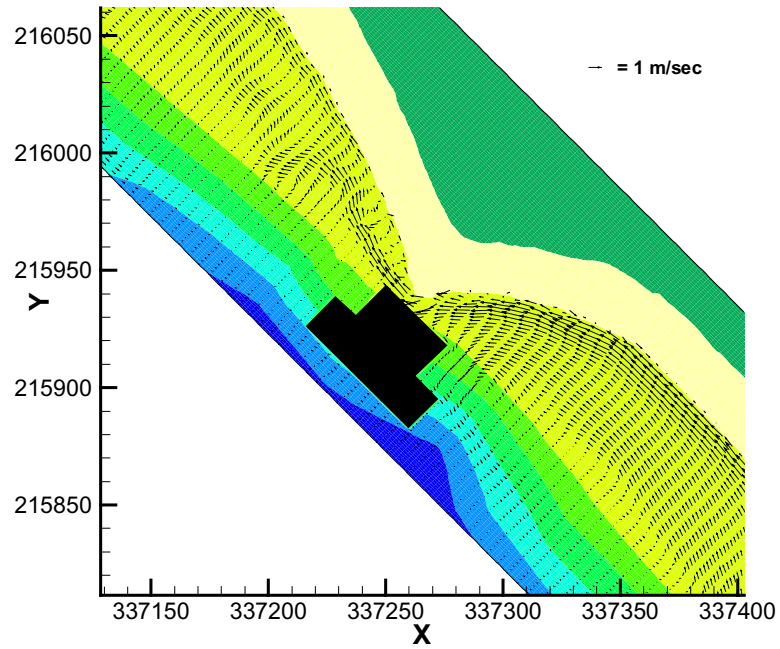


Figure 29 CoastL modeling of wave generated currents, for waves with DIR = 170 deg, H = 1 m, T = 3 sec, Tide = 0.0 m; (top) Large modeling area; (bottom) Close-up of FIL

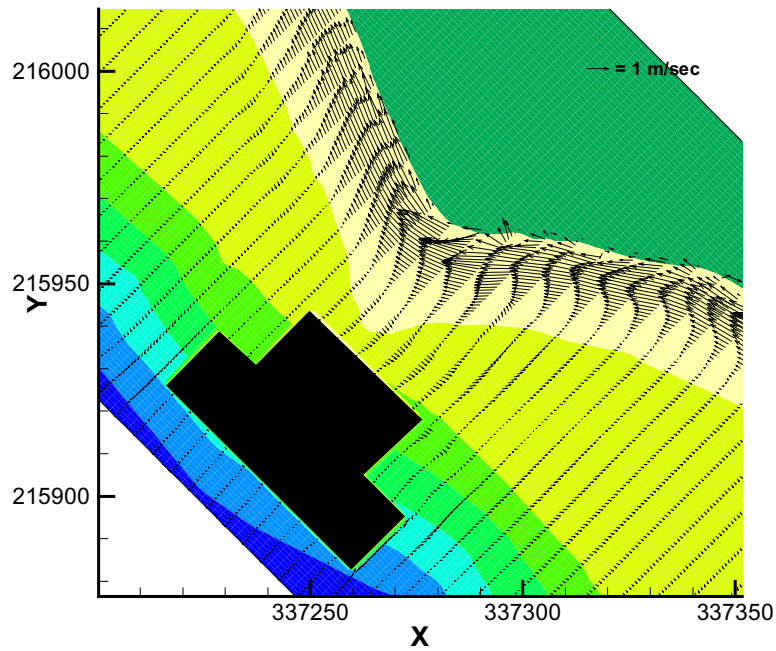
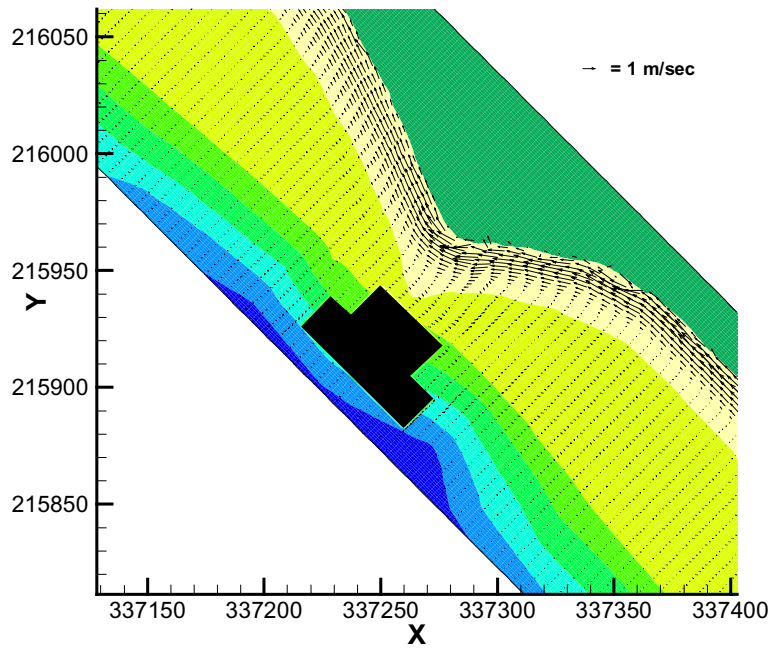


Figure 30 CoastL modeling of wave generated currents, for waves with DIR = 170 deg, H = 1 m, T = 3 sec, Tide = 3.0 m; (top) Large modeling area; (bottom) Close-up of FIL

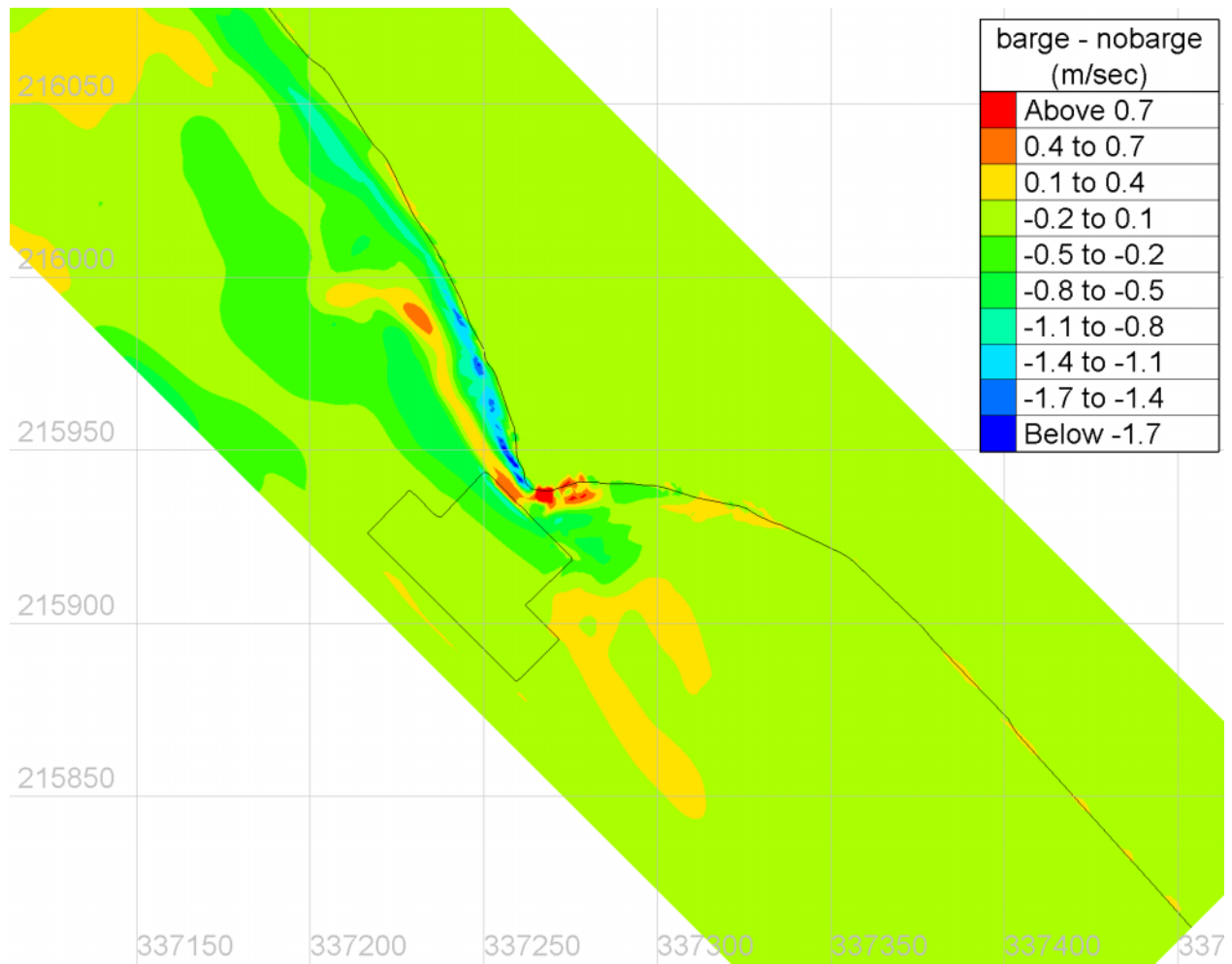


Figure 31 Wave generated current velocity differences for existing vs. no-barge conditions, for waves with DIR = 170 deg, Tide = 0.0 m

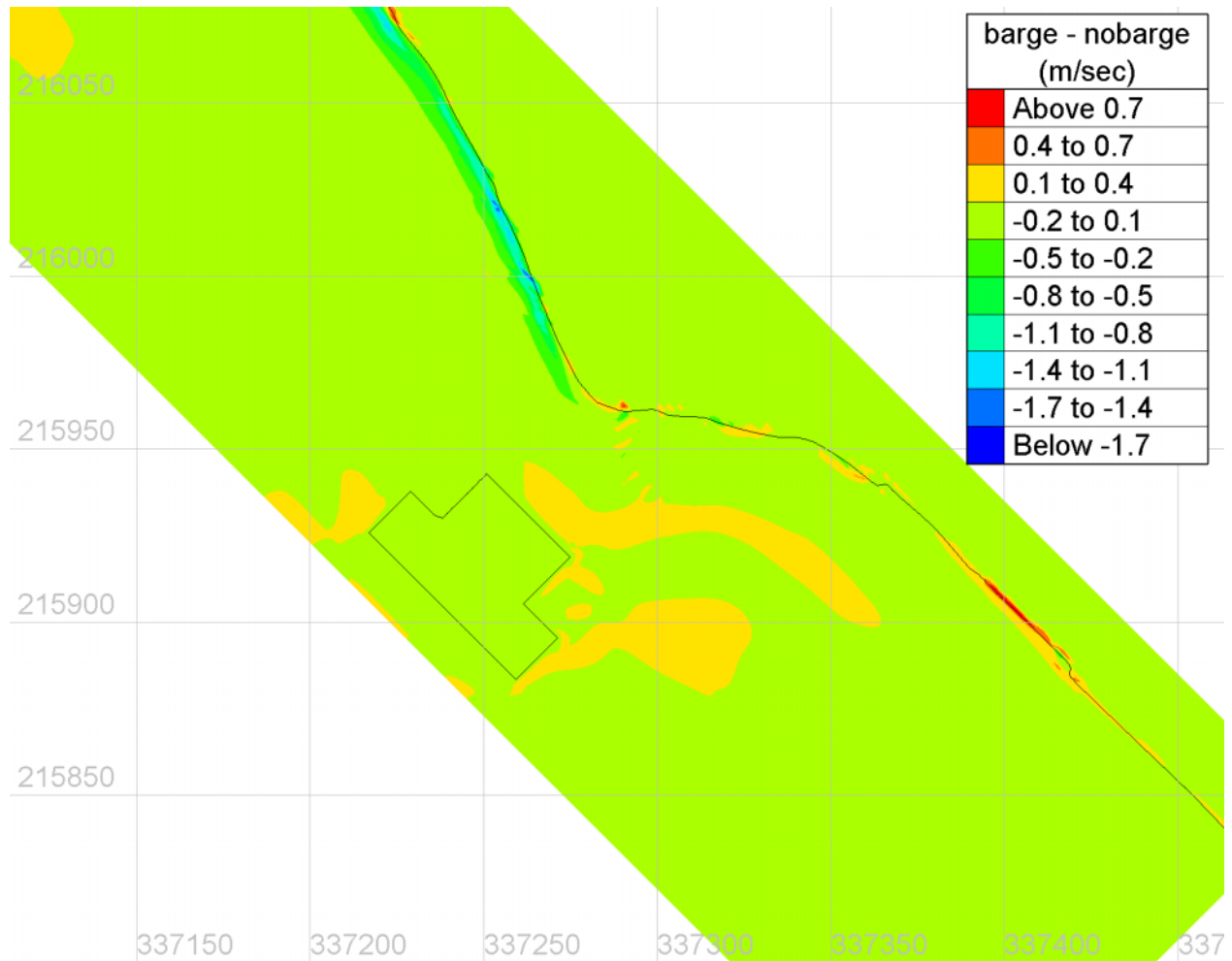


Figure 32 Wave generated current velocity differences for existing vs. no-barge conditions, for waves with DIR = 170 deg, Tide = 3.0 m

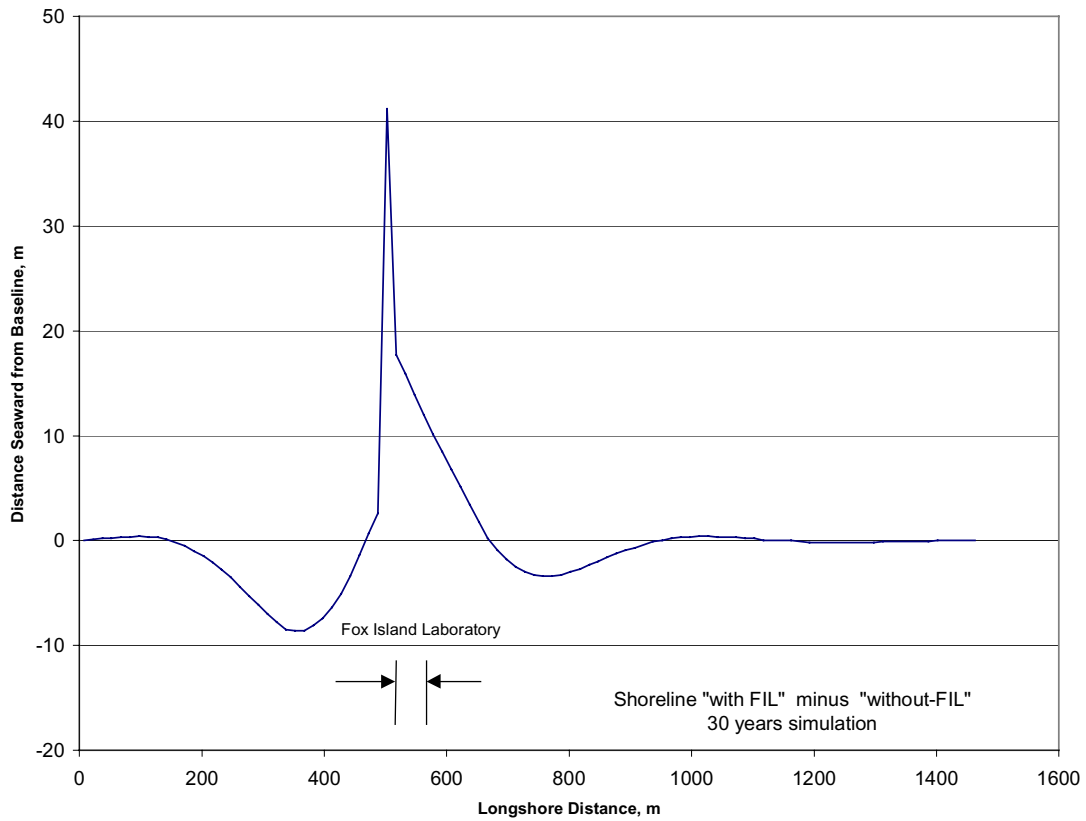


Figure 33 Comparison of shoreline change for cases “with FIL” and “without-FIL”

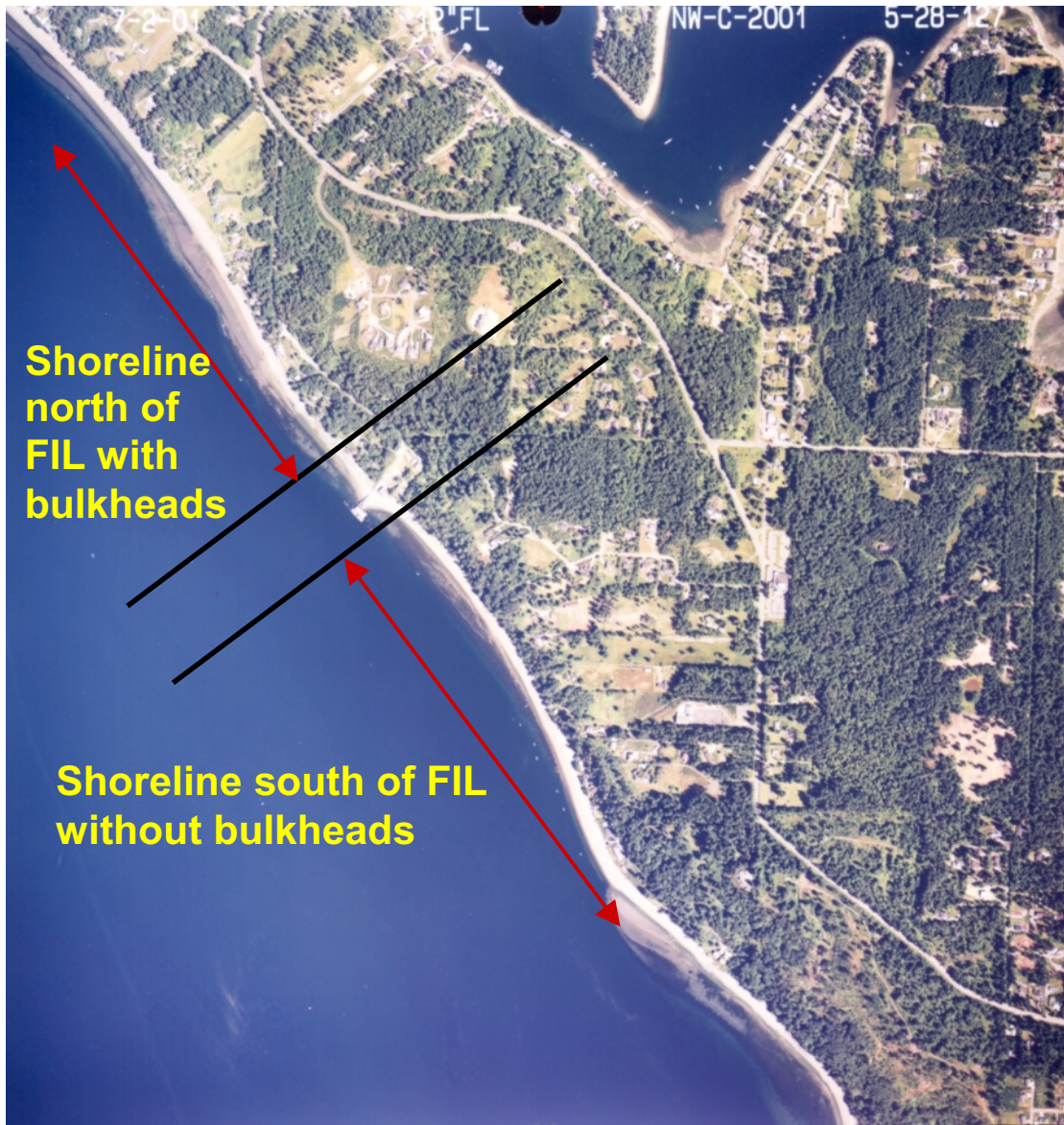


Figure 34 Character of Fox Island shoreline north and south of FIL

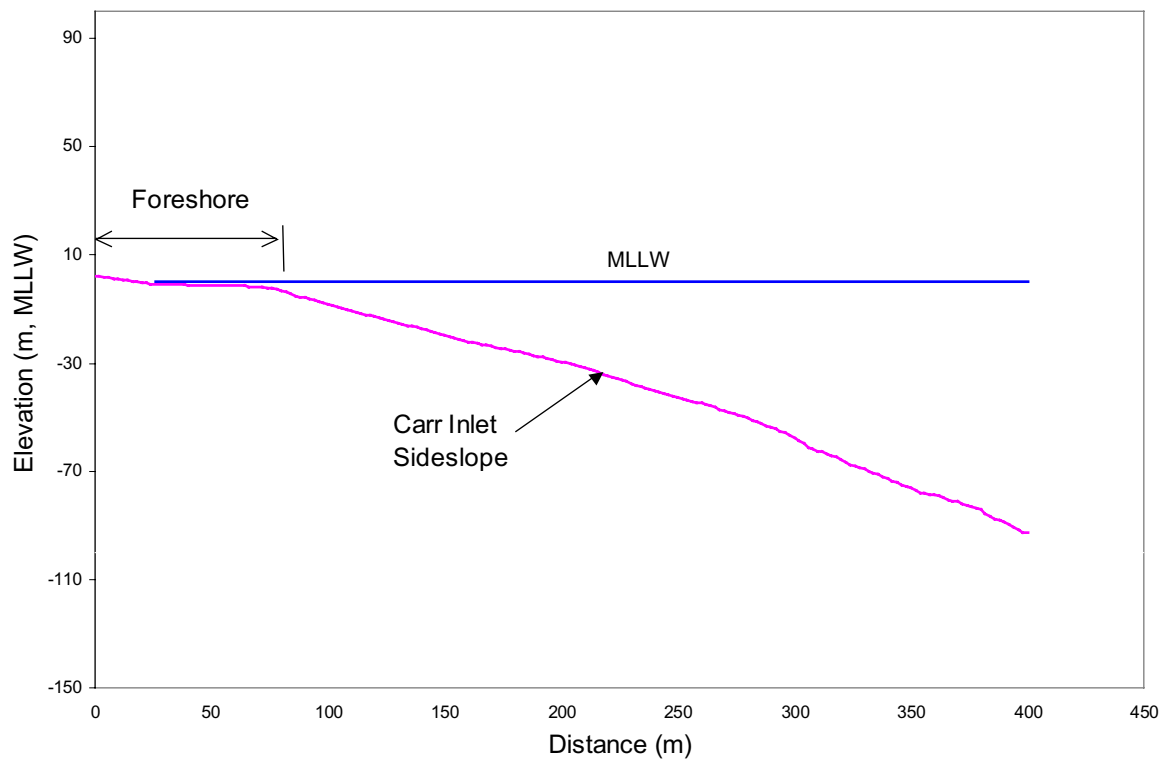


Figure 35 Typical cross-section of Fox Island shoreline north of FIL property



Figure 36 Sediment accreted near toe of bluff approximately 450 m (1,500 ft) south of FIL



Figure 37 Example of bluff toe protected from wave attack



Figure 38 Large-scale plan form of Fox Island shoreline near FIL



Figure 39 Upland slope failure at Fox Island shoreline

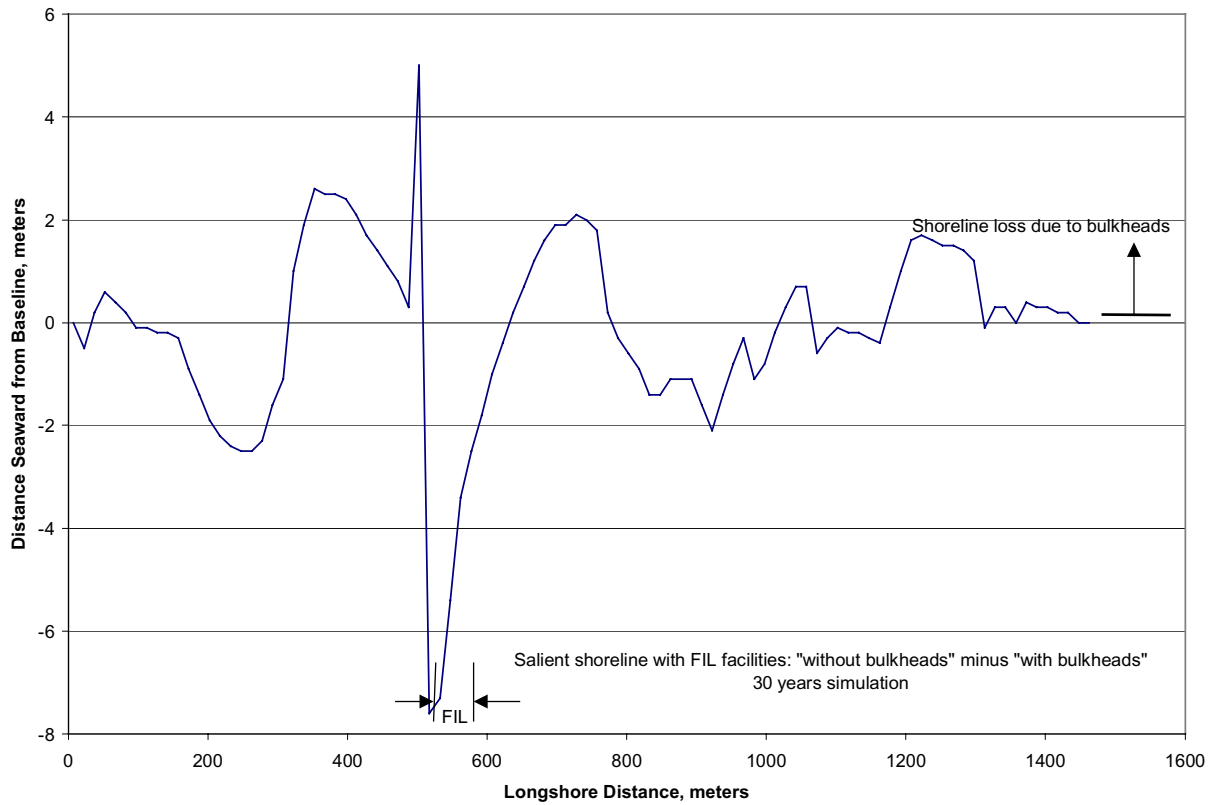


Figure 40 Comparison of shoreline change between simulations of “without bulkheads” and “with bulkheads”
 Note: FIL facilities in place for both simulations

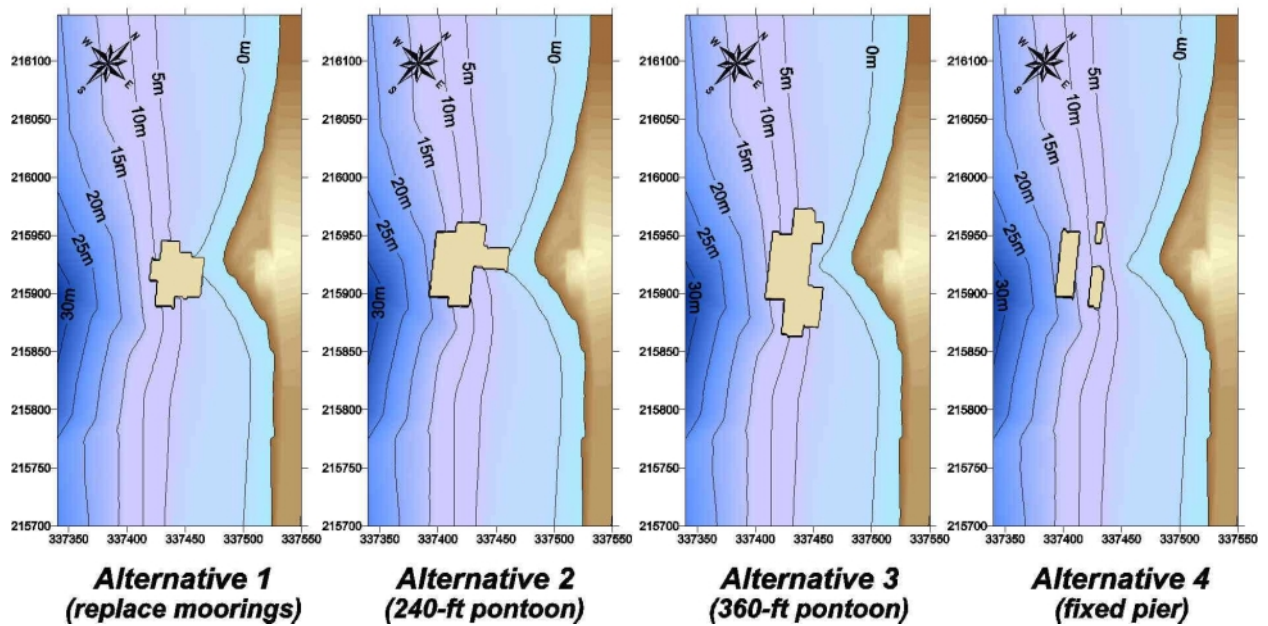


Figure 41 Bathymetry and alternative barge configurations represented in model domains

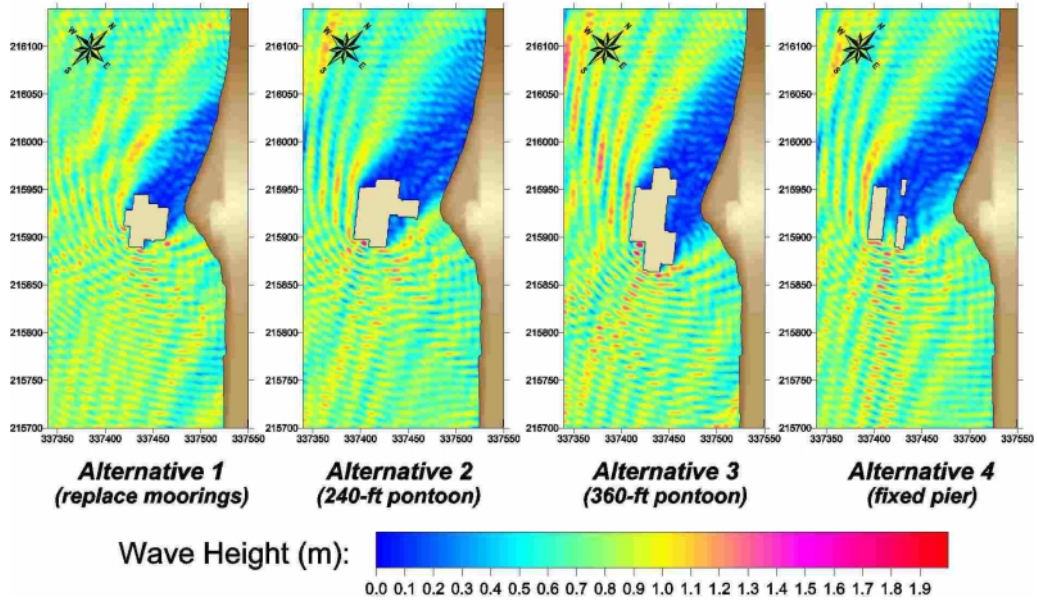


Figure 42 Wave energy blocking by alternative configuration for incident waves with $H = 0.4$ m (1.4 ft), $DIR = 170$ deg

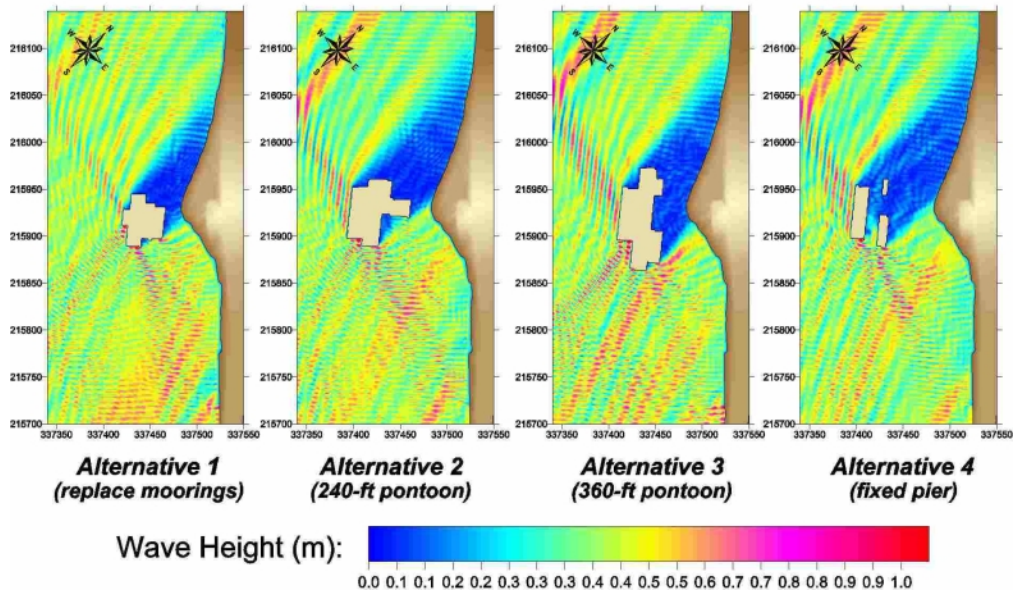


Figure 43 Wave energy blocking by alternative configuration for incident waves with $H = 0.8$ m (2.6 ft), $DIR = 170$ deg

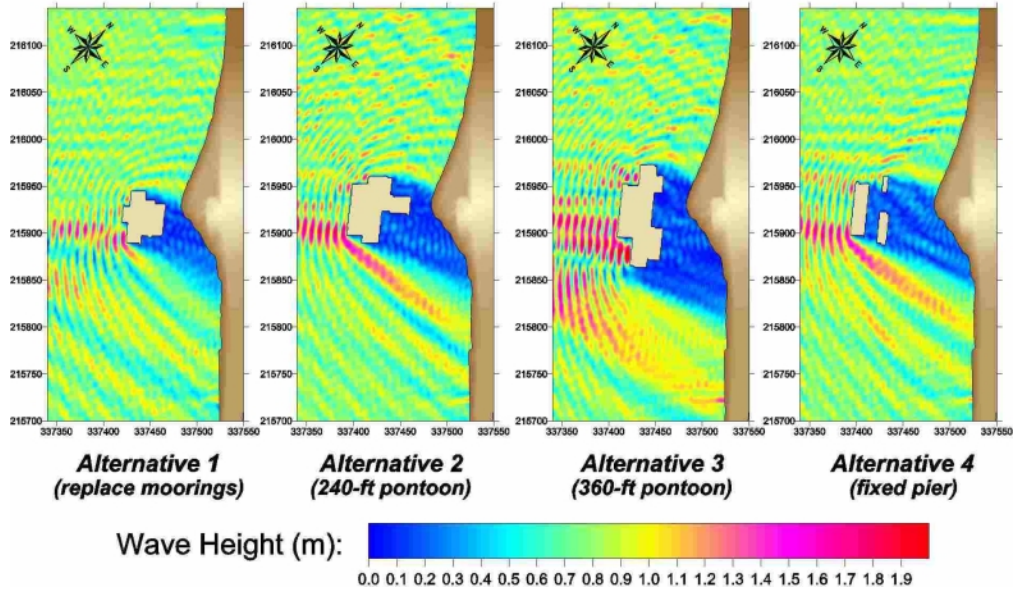


Figure 44 Wave energy blocking by alternative configurations for incident waves with $H = 0.4$ m (1.4 ft), $DIR = 250$ deg

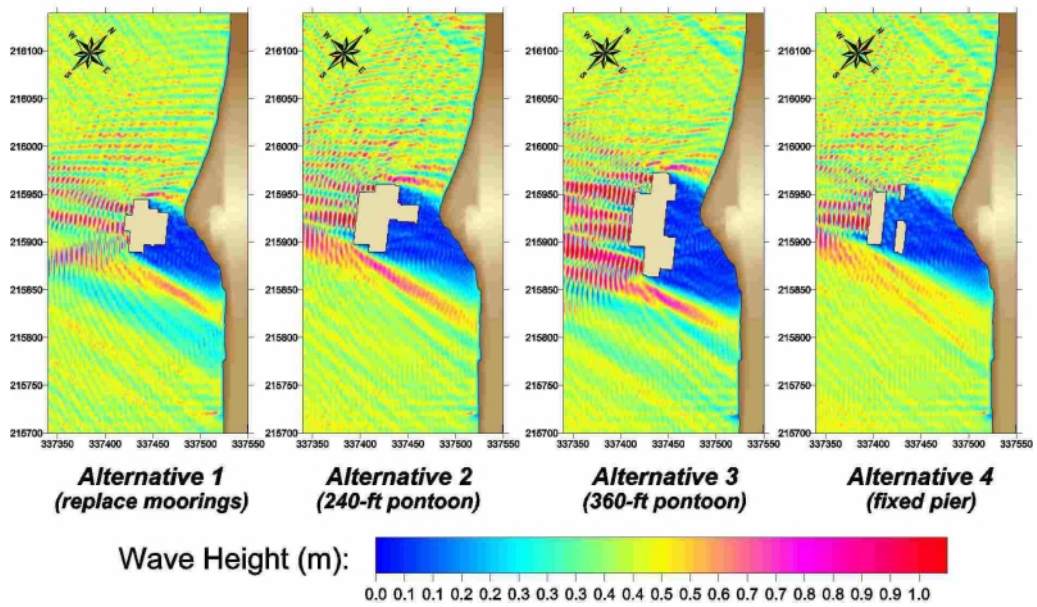


Figure 45 Wave energy blocking by alternative configurations for incident waves with $H = 0.8$ m (2.6 ft), $DIR = 250$ deg

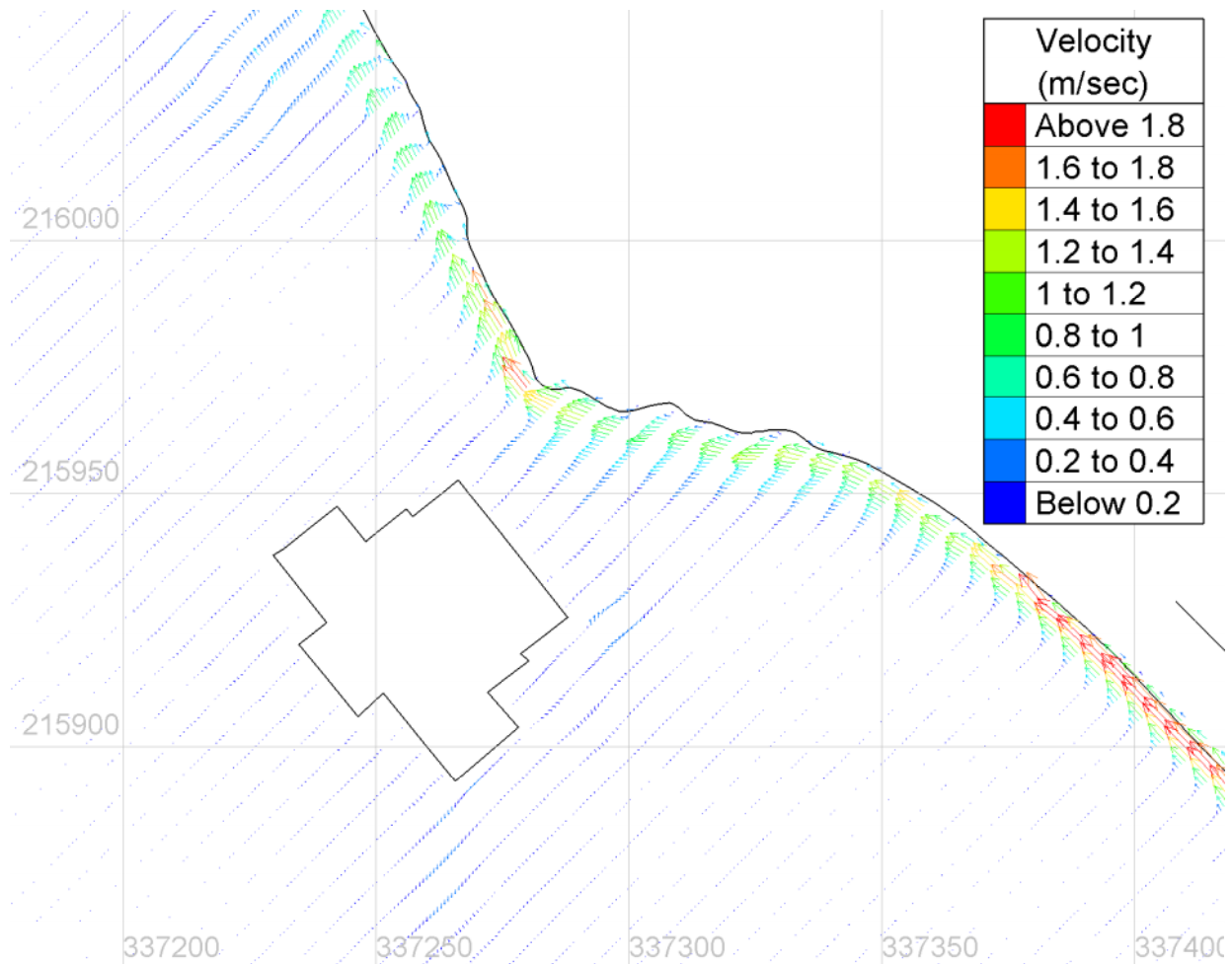


Figure 46 Longshore transport pattern, Alternative 1, for waves with $H = 0.8$ m (2.6 ft), DIR = 170 deg

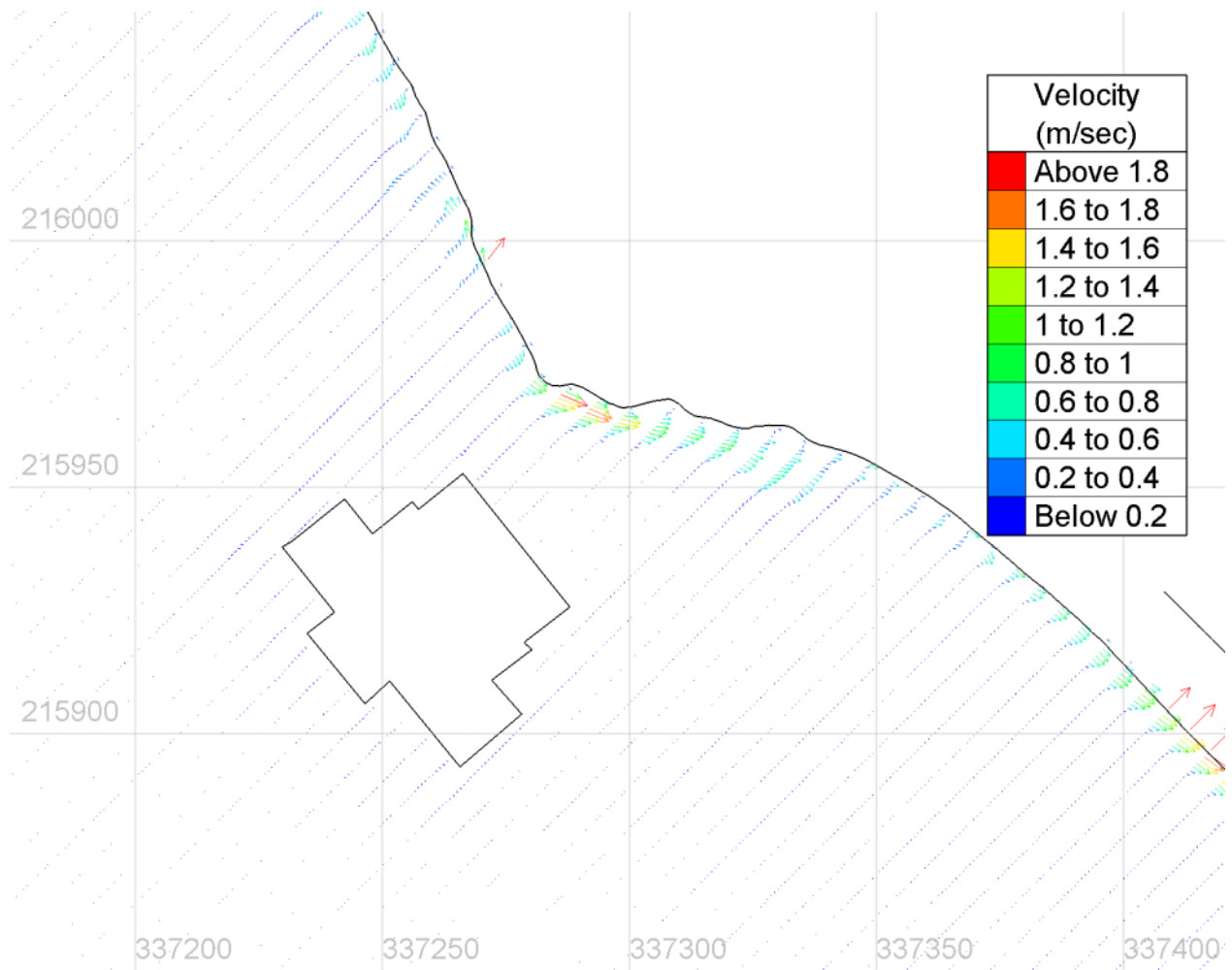


Figure 47 Longshore transport pattern, Alternative 1, for waves with $H = 0.8$ m (2.6 ft), $DIR = 250$ deg

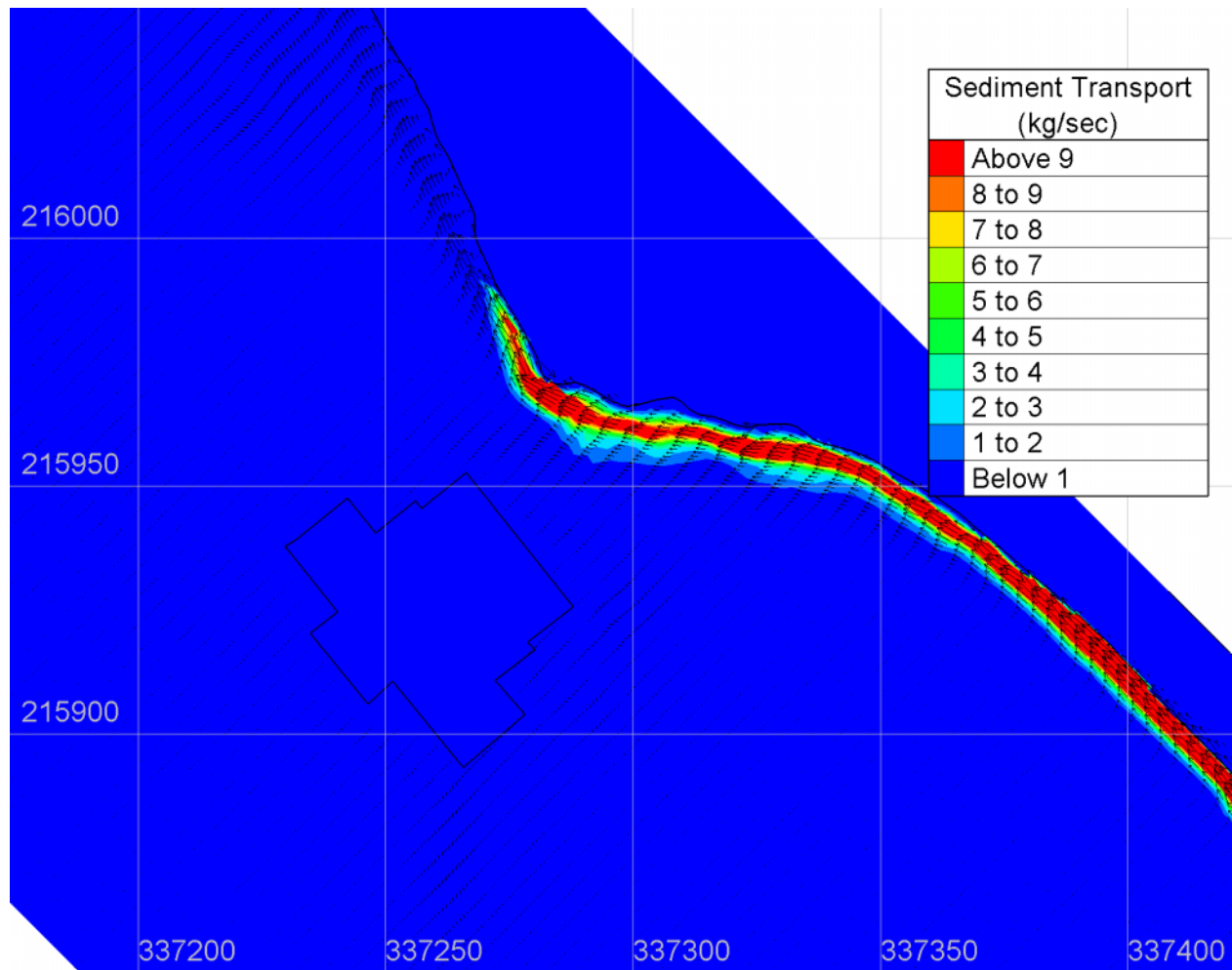


Figure 48 Transport potential under conditions of Alternative 1 and high waves from the south

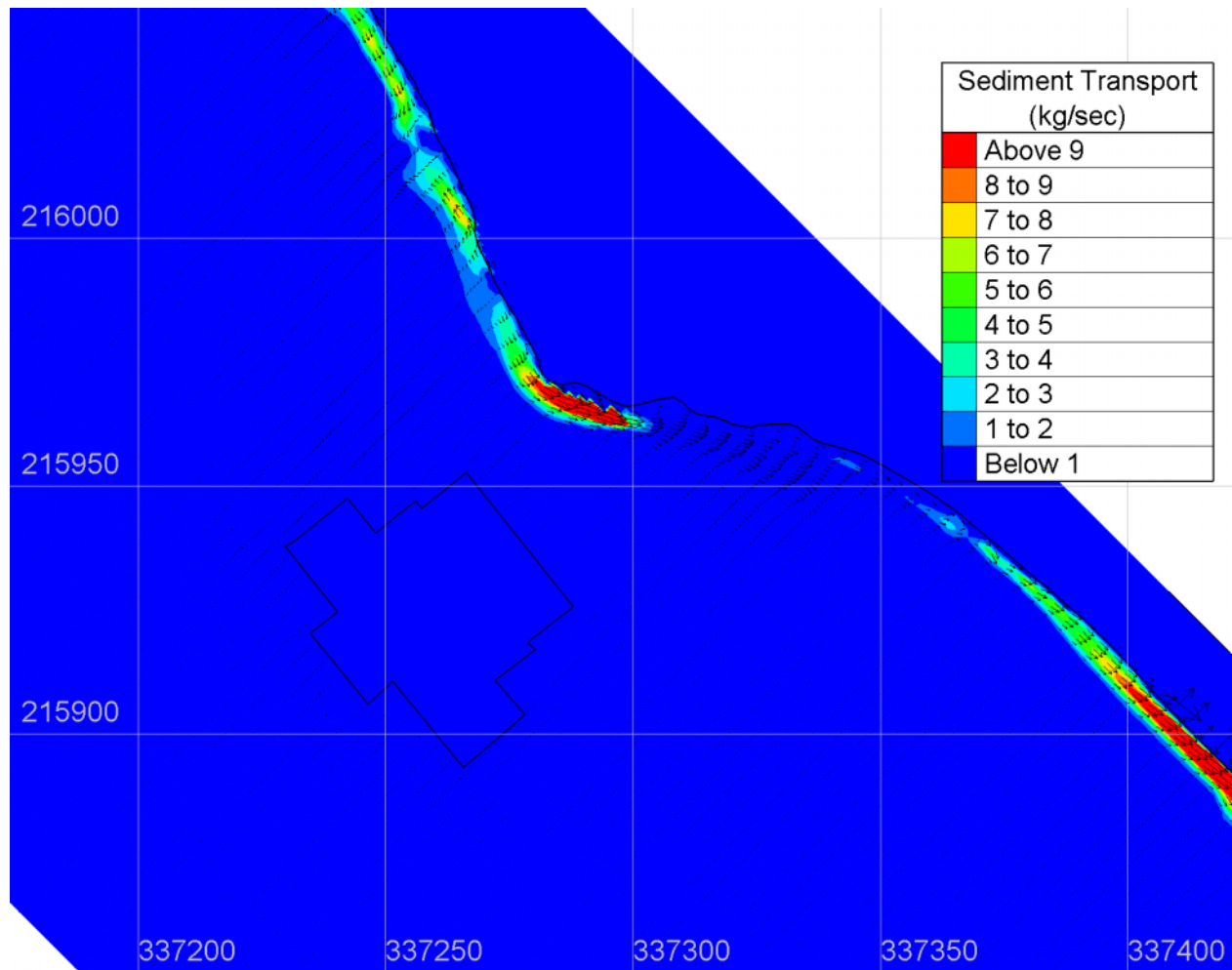


Figure 49 Transport potential under conditions of Alternative 1 and high waves from the west

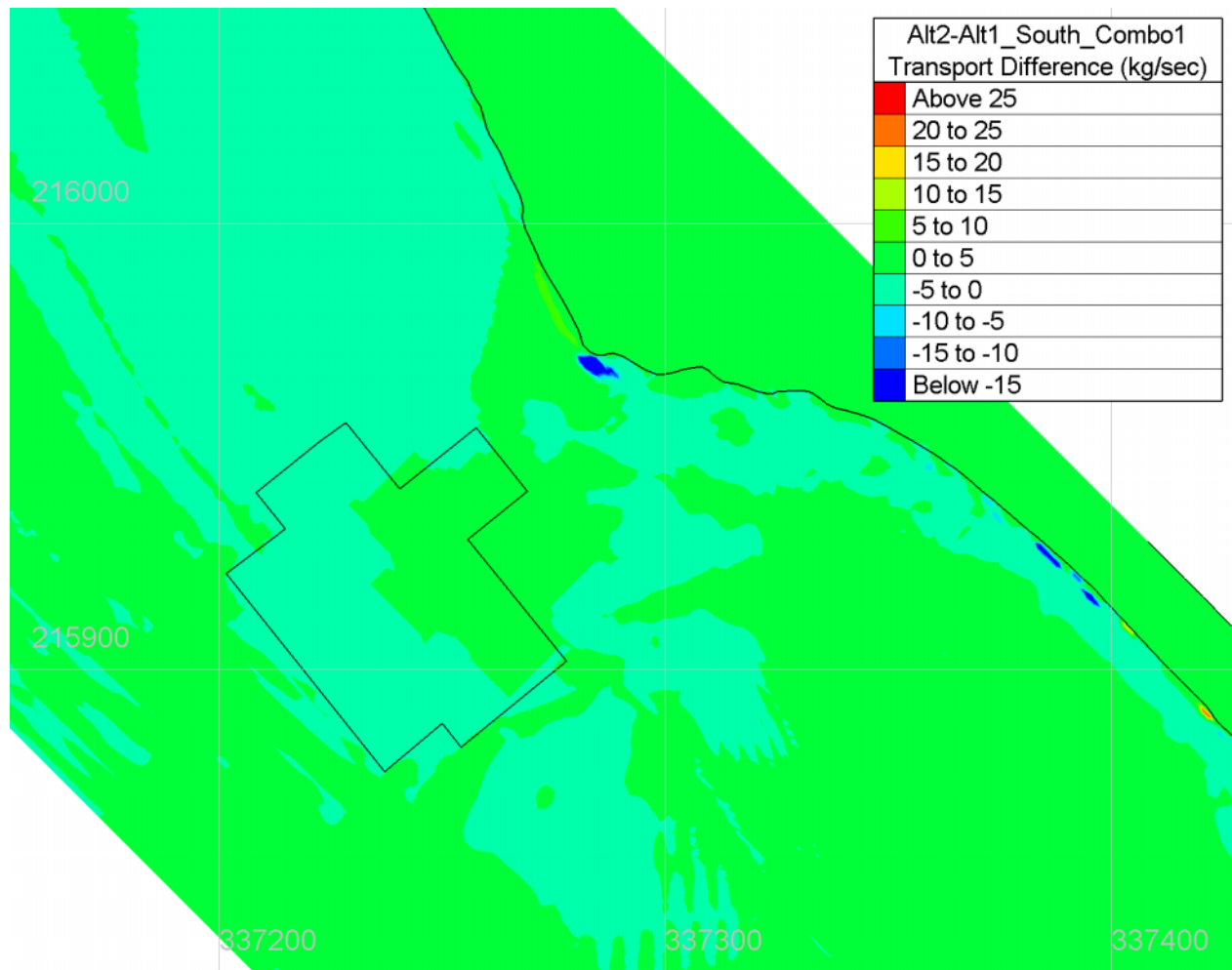


Figure 50 Potential transport difference between Alternatives 1 and 2, for waves with $H = 0.8$ m (2.6 ft), $DIR = 170$ deg

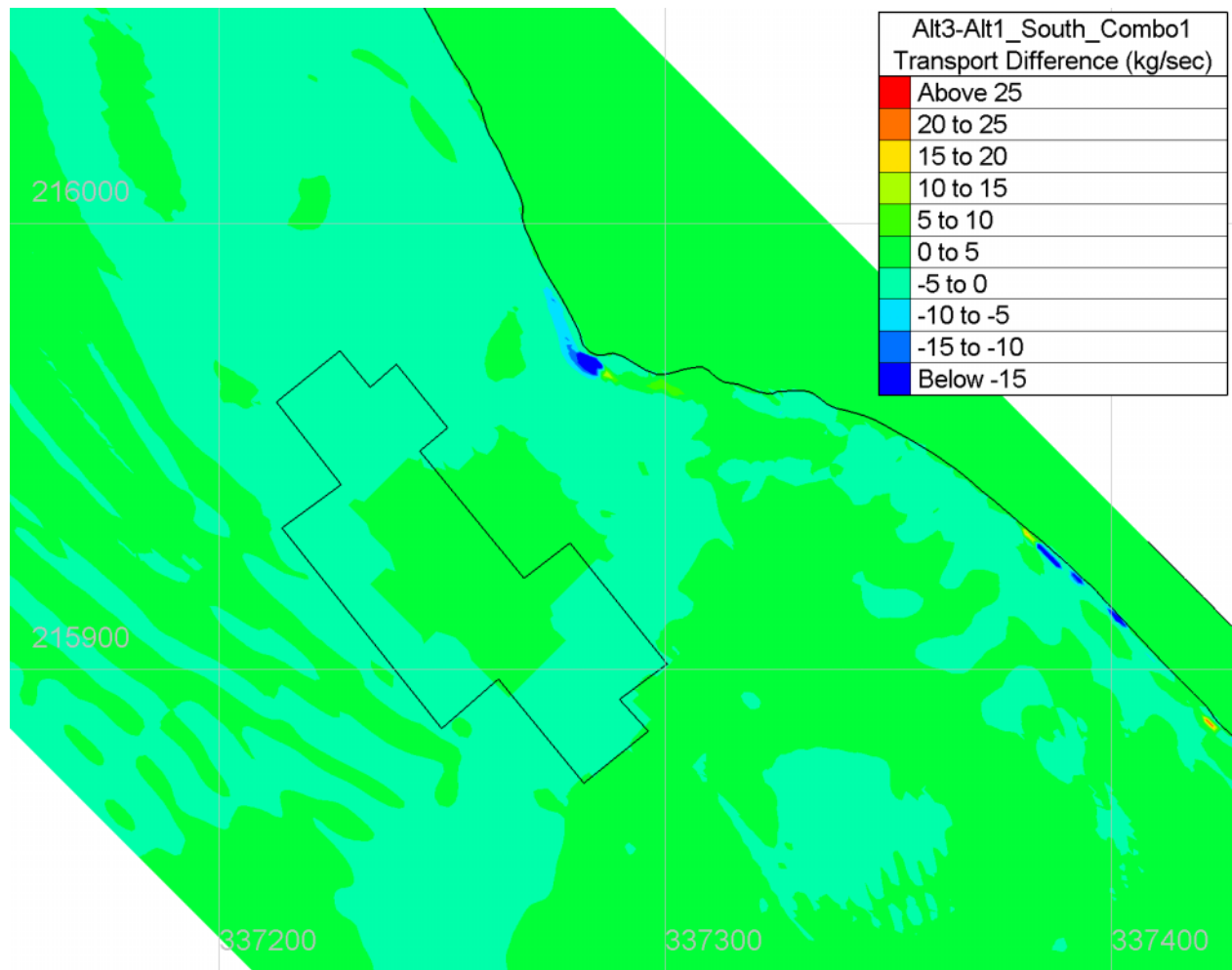


Figure 51 Potential transport difference between Alternatives 1 and 3, for waves with $H = 0.8$ m (2.6 ft), $DIR = 170$ deg

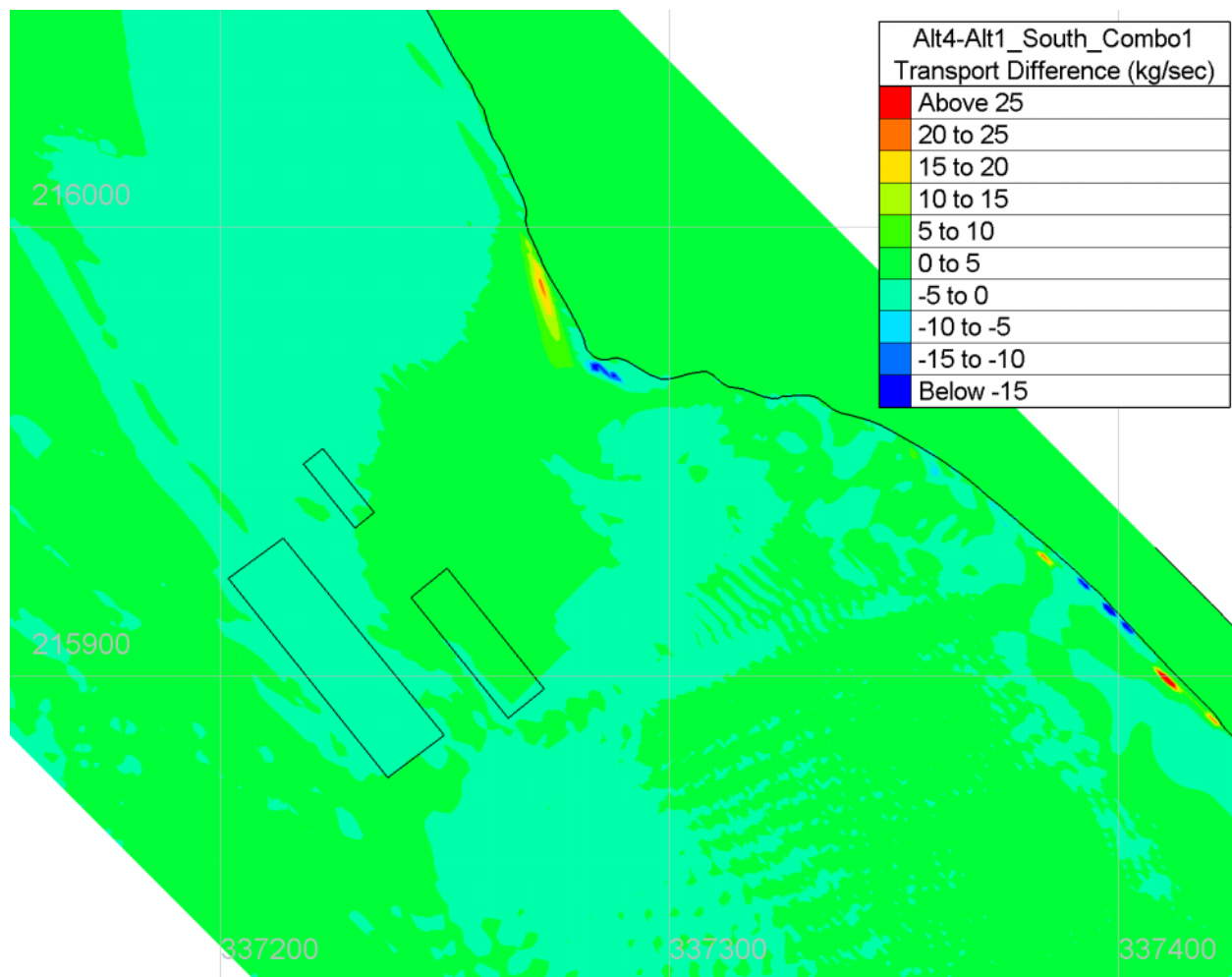


Figure 52 Potential transport difference between Alternatives 1 and 4, for waves with $H = 0.8$ m (2.6 ft), $DIR = 170$ deg

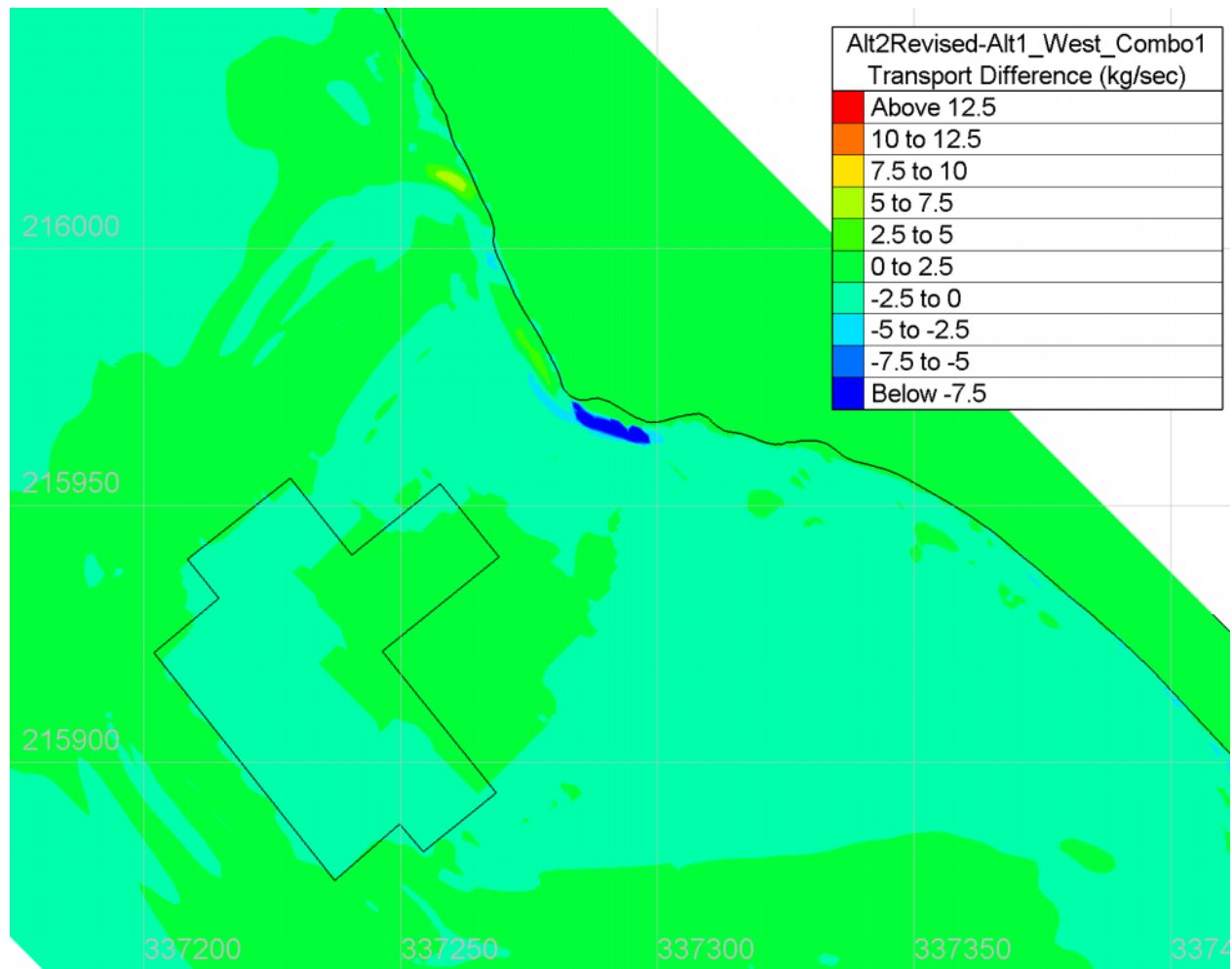


Figure 53 Potential transport difference between Alternatives 1 and 2, for waves with $H = 0.8$ m (2.6 ft), $DIR = 250$ deg

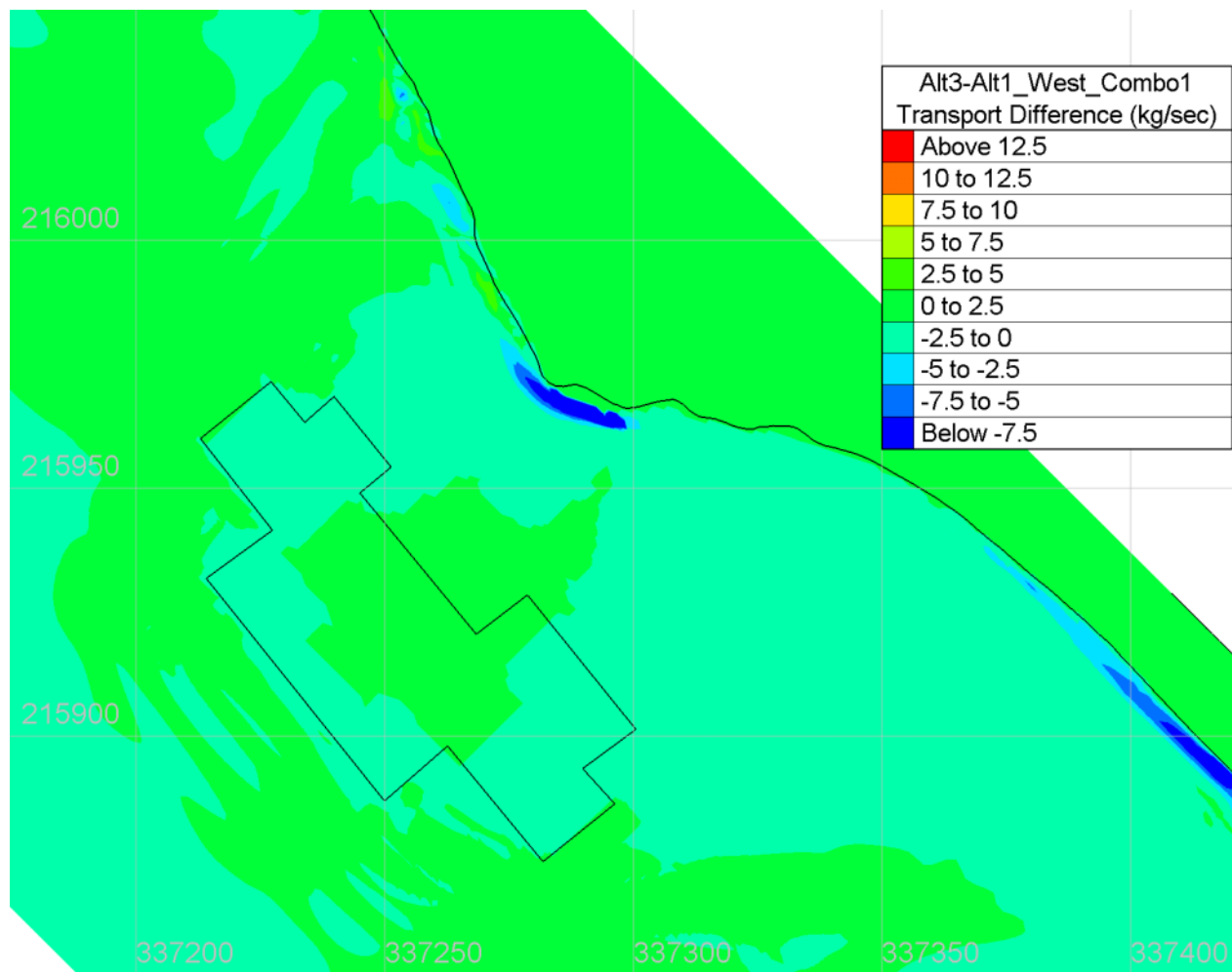


Figure 54 Potential transport difference between Alternatives 1 and 3, for waves with H = 0.8 m (2.6 ft), DIR = 250 deg

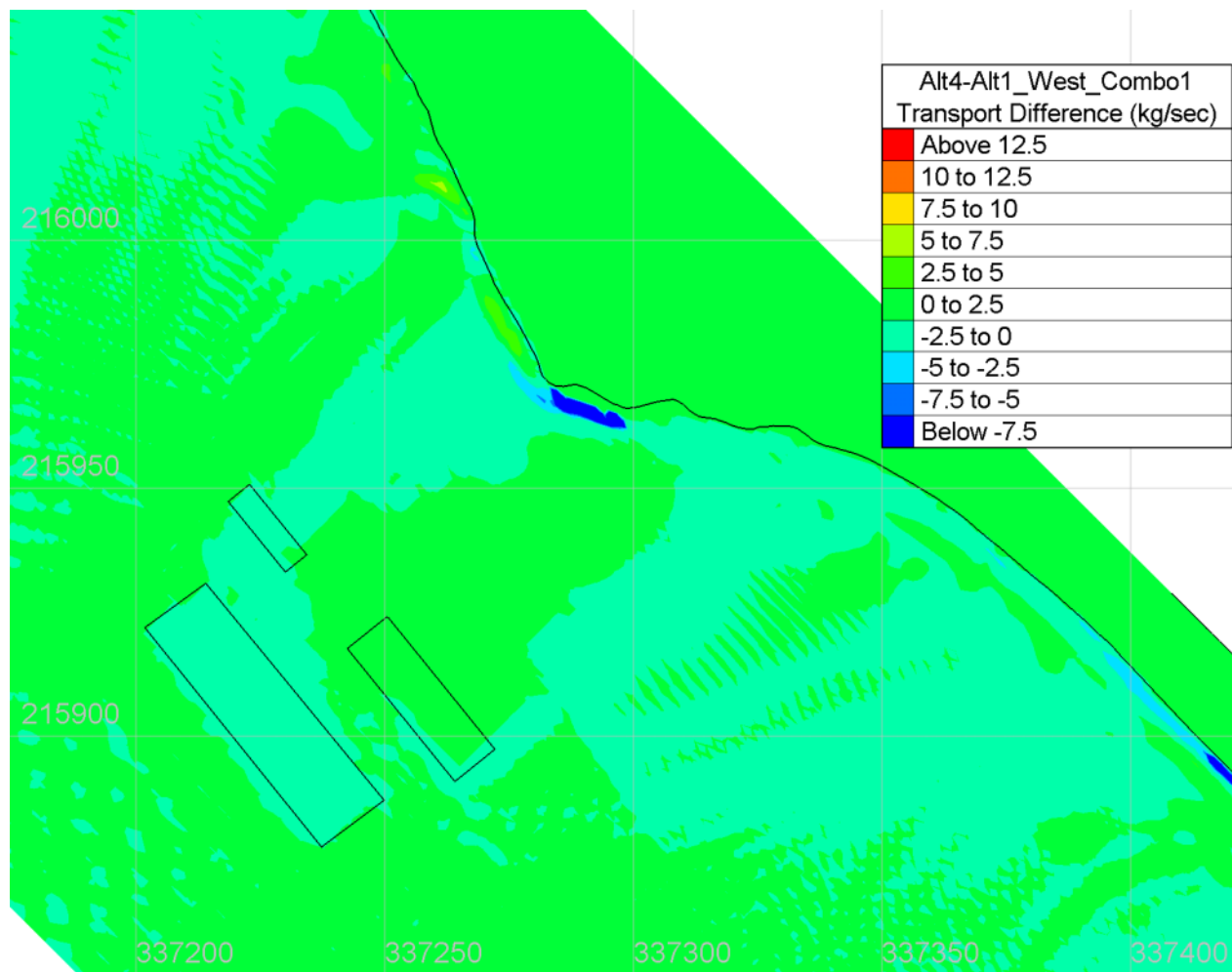


Figure 55 Potential transport difference between Alternatives 1 and 4, for waves with $H = 0.8$ m (2.6 ft), $DIR = 250$ deg

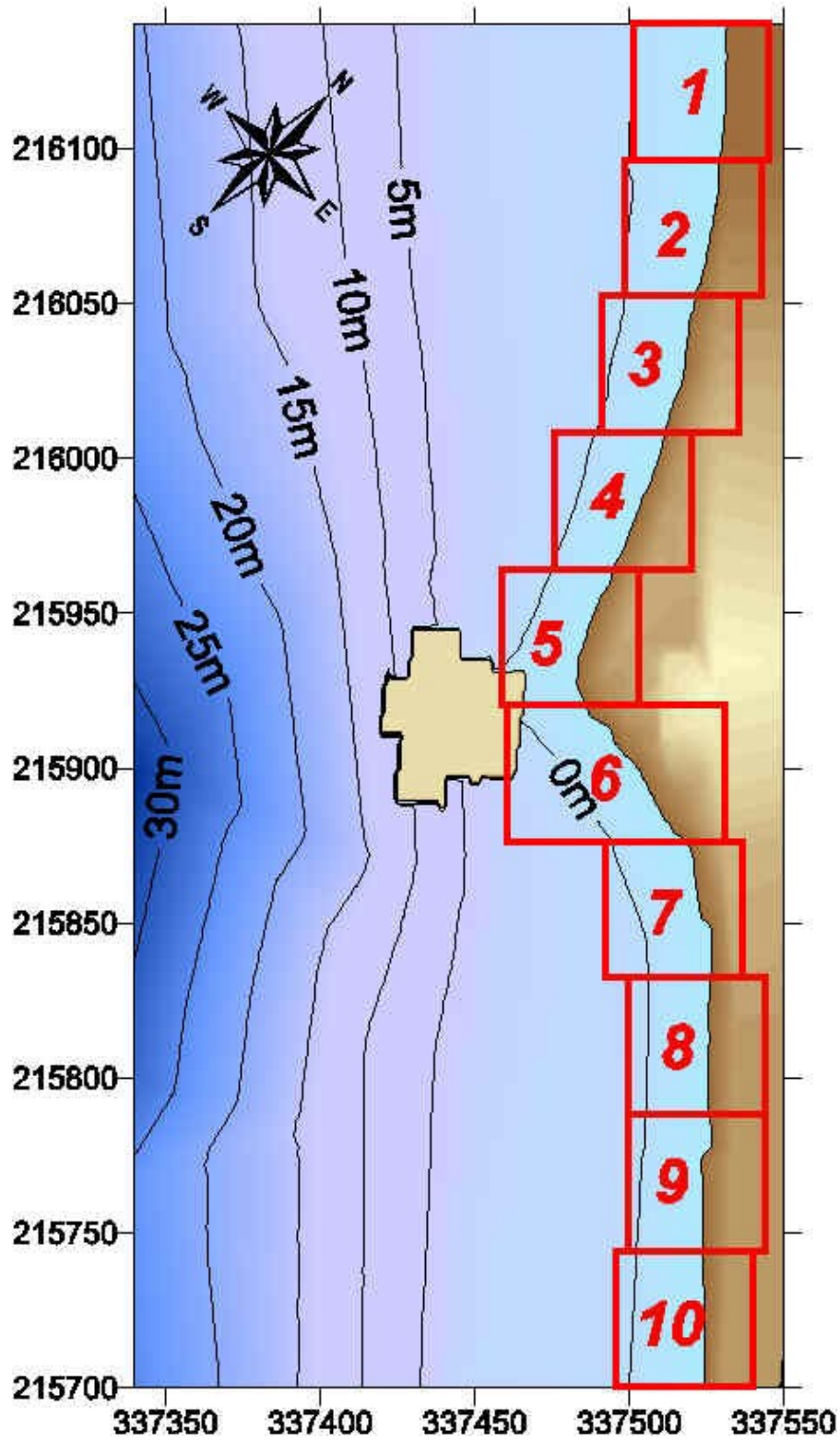


Figure 56 Areas for calculation of spatially-averaged wave-driven sediment transport